

---

## Earthquake-triggered submarine landslides in the St. Lawrence Estuary (Québec, Canada) during the last two millennia and the record of the major 1663 CE $M \geq 7$ event

Mérindol Méri1<sup>1,2,\*</sup>, St-Onge Guillaume<sup>1</sup>, Sultan Nabil<sup>2</sup>, Lajeunesse Patrick<sup>3</sup>, Garziglia Sébastien<sup>2</sup>

<sup>1</sup> Institut des sciences de la mer de Rimouski (ISMER), Canada Research Chair in Marine Geology, Université du Québec à Rimouski and GEOTOP, Canada

<sup>2</sup> Geo-Ocean UMR6538, Ifremer, CNRS, UBO, UBS, F-29280, Plouzané, France

<sup>3</sup> Département de géographie, Université Laval, Québec, Canada

\* Corresponding author : Méri1 Mérindol, email address : [meril.merindol@ifremer.fr](mailto:meril.merindol@ifremer.fr)

---

### Abstract :

In eastern Canada, the Charlevoix-Kamouraska/Bas-Saint-Laurent (CKBSL) seismic zone presents a seismic hazard almost as high as that of the active Pacific zone. The major event of February 5, 1663 CE, with an estimated magnitude of  $\geq 7$ , highlights the importance of this seismic hazard. The numerous submarine landslides mapped in the St. Lawrence Estuary in the CKBSL seismic zone suggest that earthquakes triggered series of submarine slope failures. In this context, the SLIDE-2020 expedition on board the RV Coriolis II in the St. Lawrence Estuary aimed to map, image and sample more than 12 zones of submarine instabilities and their associated deposits. The analysis of sediment cores sampled in the distal sedimentary deposits from these landslides reveals the presence of rapidly deposited layers (turbidites, hyperpynites and debrites) directly linked to the submarine landslides. Dating these landslides with <sup>210</sup>Pb and <sup>14</sup>C techniques led to the identification of four periods of synchronous submarine landslides corresponding to the strongest historical earthquakes: 1663 CE, 1860/1870 CE, 1925 CE and 1988 CE ( $M \geq 7$ ,  $M = 6.1/6.6$ ,  $M = 6.2$ ,  $M = 5.9$ ). This synchronicity over a distance reaching 220 km of several landslides supports a relationship between their triggering in the St. Lawrence Estuary and regional seismicity. The fact that as many as nine submarine landslides appear to have been triggered by the 1663 CE earthquake suggests that this event is the strongest recorded in the last two millennia in the region.

### Highlights

► Submarine landslides distributed over 220 km in the St. Lawrence Estuary were dated. ► Submarine landslide deposits are synchronized to major historical earthquakes. ► Two older coeval submarine landslide deposits were dated around 645 and 1145 CE ► The 1663 CE event appears to be the strongest earthquake of the last 2000 years.

---

**Keywords** : 1663 CE earthquake, Canada, Geohazards, Geophysics, Holocene, Quebec, Paleoseismicity, Sedimentology, Submarine landslides, Turbidites

## 29 1. Introduction

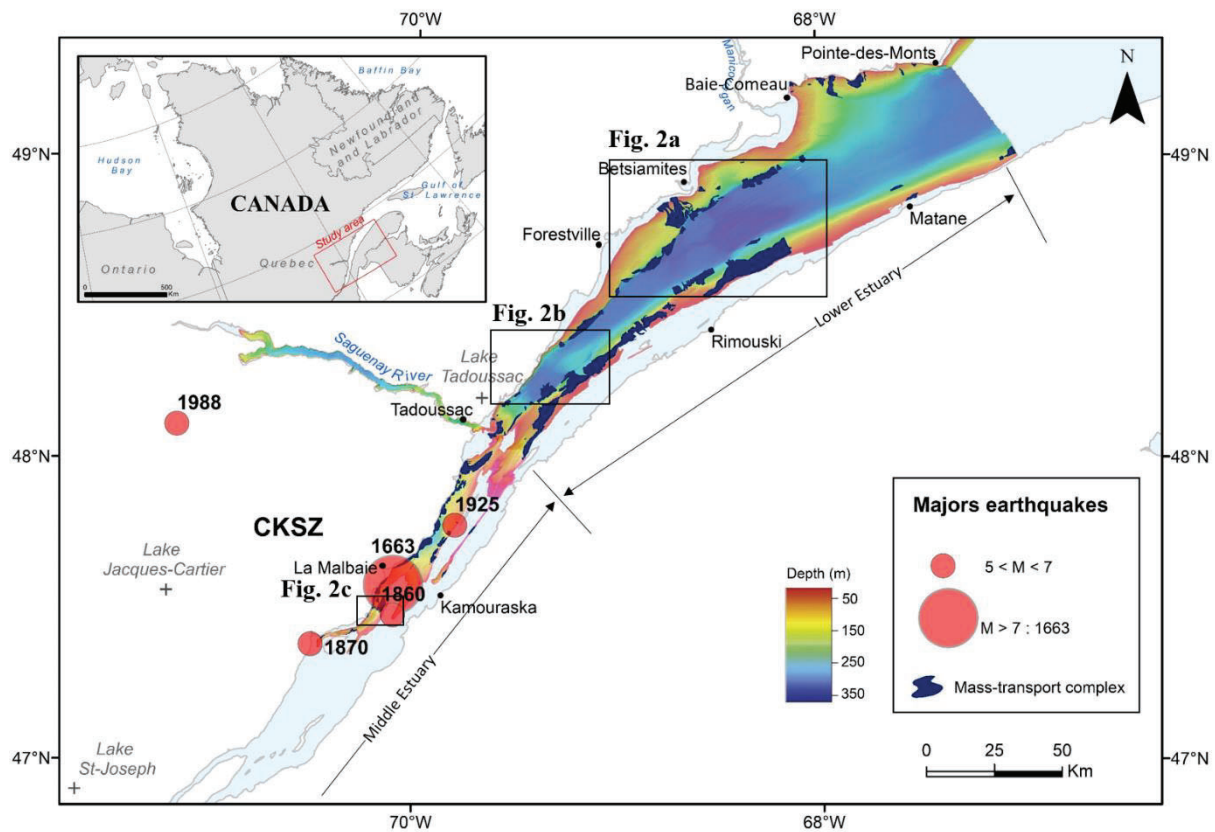
30 One of the strongest historical earthquakes felt in eastern North America occurred on February 5, 1663,  
31 along the St. Lawrence River, in southern Québec, Canada, when the region was sparsely inhabited and  
32 the European settling was at its beginning. Therefore, the precise epicenter and magnitude of this event  
33 are estimated only from written and personal accounts of the event (Gouin, 2001). Previous studies  
34 converge to indicate that its epicenter was located in the Charlevoix-Kamouraska seismic zone (CKSZ),  
35 in the western part of the St. Lawrence Estuary (**Fig. 1**), although its exact localisation is still debated  
36 (Hodgson, 1928; Locat, 2011; Locat *et al.*, 2003; Locat *et al.*, 2016; Pinet *et al.*, 2021). Gouin (2001)  
37 has compiled testimonies of damage to barns, chimneys and houses in eastern America in an area  
38 reaching 600 km around the suspected epicenter. From this historical data, Ebel (2011) estimated the  
39 magnitude (M) of the 1663 earthquake at 7.5 while the Canadian catalog of historical earthquakes, used  
40 to map the seismic hazard in Canada, considers a magnitude slightly lower, of  $M = 7$  (Smith, 1962;  
41 Lamontagne *et al.*, 2018).

42 Jesuits writings contemporary to the 1663 CE earthquake (e.g., Ebel, 1996) report “the formation of new  
43 lakes”, “the disappearance of mountains” and “the displacement of forest down to the St. Lawrence  
44 River” as consequences of subaerial landslides most likely triggered by the 1663 earthquake. The  
45 historical observations are consistent with studies carried out on regional landslides which established a  
46 link between the 1663 CE earthquake and the landslides observed at Saint-Jean-Vianney (Lasalle and  
47 Chagnon, 1968), the Gouffre River (Filion *et al.*, 1991), the Mont-Eboulé (Dubé, 1998) and Colombier  
48 (Cauchon-Voyer *et al.*, 2008). The recent study conducted in the CKSZ (**Fig. 1**) by Pinet *et al.* (2015),  
49 indicates that more than one hundred submarine mass-movements occurred in the St. Lawrence Estuary.  
50 The high density of submarine landslides in the CKSZ suggests a possible link between submarine slope  
51 destabilization and seismicity (e.g., Cauchon-Voyer *et al.*, 2008; Campbell *et al.*, 2008). Some  
52 submarine landslides have been related to regional seismicity such as in the Betsiamites River area,  
53 where Cauchon-Voyer *et al.* (2008, 2011) combined terrestrial and marine data to relate submarine  
54 landslides to major earthquakes occurring before 9280 cal yr BP, in 7250 cal yr BP and in 1663 CE.  
55 Other authors have observed this relationship in Québec using geomorphological, sedimentological and

56 dating methods but outside the St. Lawrence Estuary such as in the Saguenay Fjord (Syvitski and  
57 Schafer, 1996; Locat *et al.*, 2003; St-Onge *et al.*, 2004) and in lacustrine environments (Doig, 1990;  
58 Ouellet, 1997; Locat *et al.*, 2016; Trottier *et al.*, 2018).

59 Submarine landslides, through erosion of the seafloor and incorporation of sediments and water, can  
60 evolve into a debris flow and a turbidity current (Bryn, 2005; Strachan, 2008). Over the last two decades,  
61 the marine turbidite record has been increasingly used as a proxy for earthquake recurrence (Lebreiro *et*  
62 *al.*, 1997; Gracia *et al.*, 2010; Goldfinger *et al.*, 2012; St-Onge *et al.*, 2012; Ratsov *et al.*, 2015; Piper *et*  
63 *al.*, 2019; Howarth *et al.*, 2021). The recurrence of strong regional earthquakes and the risks they pose  
64 when associated with submarine slope failures can have major impacts on coastal environments (e.g.,  
65 damage to coastal infrastructures and threats to coastal communities, risk of tsunamis, cable rupture,  
66 coastal erosion), particularly with increasing human populations along the coast. It is therefore essential  
67 to improve our knowledge of natural hazards by establishing a chronology of submarine landslides  
68 triggered by earthquakes.

69 Mapping and dating of submarine landslides at a regional scale provide the opportunity to assess their  
70 synchronicity and thus their possible triggering by an earthquake (Goldfinger *et al.*, 2012, 2018; Patton  
71 *et al.*, 2015). This paper involves 19 sediment cores recovered near 12 submarine landslides located over  
72 a distance of ~220 km in the St. Lawrence Estuary with the aim of: (1) identifying and characterizing  
73 rapidly deposited layers (RDLs) resulting from landslides (e.g., debrite, turbidite) dated by radiocarbon  
74 and  $^{210}\text{Pb}$ ; and (2) relate them to historical earthquakes (**Fig. 1**).



75  
 76 **Fig. 1.** Bathymetric map of the St-Lawrence Estuary and location of significant East Canadian  
 77 Earthquakes of the period 1663-2005 (red circles) from Lamontagne *et al.* (2018). Dark blue areas  
 78 indicate the mass-transport complexes mapped by Pinet *et al.* (2015). CKSZ corresponds of the  
 79 Charlevoix-Kamouraska Seismic Zone.

## 80 2. Regional setting

### 81 2.1. The St. Lawrence Estuary (Eastern Canada)

82 The St. Lawrence Estuary, located in Québec (eastern Canada), is one of the world's largest estuarine  
 83 basins (~8 000 km<sup>2</sup>). It is generally considered to be divided into two parts: the Lower Estuary, from the  
 84 mouth of the Saguenay River to Pointe-des-Monts, and the Middle Estuary, upstream and southwest of  
 85 the Saguenay River (**Fig. 1**) (e.g., Pinet *et al.*, 2011). The maximum water depth of 355 m is reached in  
 86 the central part of the estuary, in the Laurentian Channel, where the seafloor presents a sub-horizontal  
 87 depression ~900 km long. This major feature is a U-shaped incised-valley bounded by steep escarpments  
 88 inherited from Quaternary glacial successive erosions (Josenhans and Lehman, 1999; Shaw *et al.*, 2002)

89 and phases of preglacial subaerial erosion (King and MacLean, 1970). In the Lower Estuary, its  
 90 topography is mostly shaped by mass-transport deposits and pockmarks (Locat *et al.*, 2004; Pinet *et al.*,  
 91 2008). In this study, six regions with submarine landslides were considered representing the estuary over  
 92 its entire length (**Fig. 1** and **Table 1**). The Rimouski, Baie-Comeau and Betsiamites sectors are located  
 93 in the eastern part of the Lower Estuary and the Forestville and Saguenay sectors are located in its  
 94 western part. Only the La Malbaie area is located in the Middle Estuary.

95 **Table 1.** Location and length of the studied cores.

Area and core name	Zone	Lat. (°N)	Long. (°W)	Length (m)
<i>Rimouski</i>				
COR20-02-03GC	Slope	48°34.71	68°29.66	3.87
<i>Baie-Comeau</i>				
COR20-02-13GC	Slope - Deposit	48°58.71	68°10.74	4.20
COR20-02-14GC	Deposit	48°57.94	68°12.25	3.87
<i>Betsiamites</i>				
COR20-02-17GC	Deposit	48°53.27	68°29.93	3.45
COR20-02-18GC/BC	Deposit	48°50.97	68°32.10	3.97
COR20-02-04GC	Lobe	48°34.77	68°29.76	3.86
COR07-03-11PC	Deposit	48°48.58	68°38.34	2.45
COR07-03-13PC	Scar	48°51.10	-68°37.24	4.09
COR20-02-19GC	Deposit	48°48.37	68°37.30	2.32
<i>Forestville</i>				
COR20-02-20GC/BC	Deposit	48°27.96	69°10.04	5.05
COR20-02-21GC	Deposit	48°21.14	69°08.47	2.49
<i>Saguenay</i>				
COR20-02-26GC/BC	Deposit	48°12.25	69°31.87	2.83
COR20-02-28GC/BC	Deposit	48°12.88	69°25.87	1.01
COR20-02-29GC	Deposit	48°11.82	69°27.40	1.60
<i>La Malbaie</i>				
COR20-02-50GC	Deposit	47°30.72	70°10.84	2.28

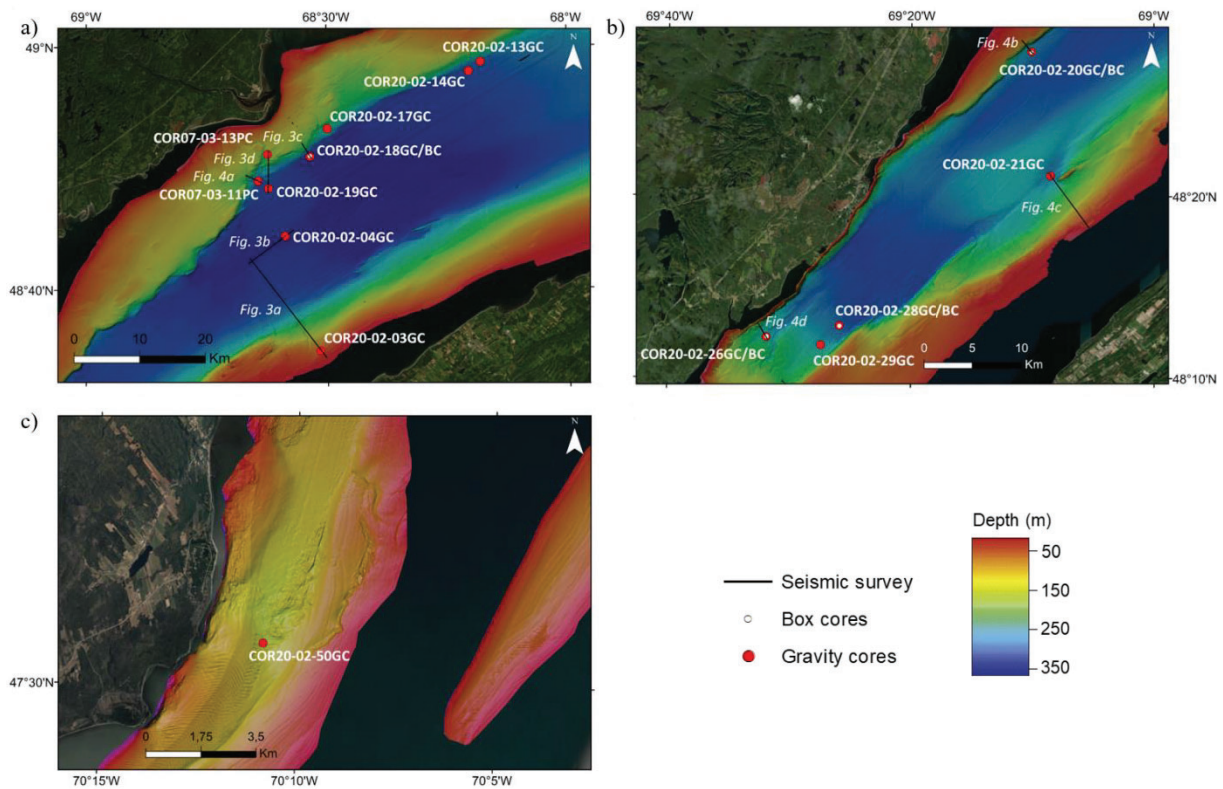
96 The basement of the St. Lawrence Estuary is mostly composed of carbonate and siliciclastic rocks from  
 97 the St. Lawrence Platform (Duchesne *et al.*, 2007). It is predominantly covered by Quaternary  
 98 sediments, except in narrow strips at Anticosti and Mingan (Haworth, 1978). The St. Lawrence Platform  
 99 is bordered to the north by the Grenville Formation, composed of metamorphic rocks, and to the south  
 100 by the Appalachian Mountains, composed of Paleozoic sedimentary rocks (e.g., Duchesne *et al.*, 2007).  
 101 Less resistant to erosion, the Laurentian Channel is parallel to these two formations (Pinet *et al.*, 2008).

102 The estuary is divided into three physiographic regions: the shelf, the slope and the Laurentian Channel.  
103 In the Middle Estuary, the shelf is reduced and even absent (**Fig. 1-2**).  
104 Inputs of sediments to the estuary originate from five main rivers in addition to the St. Lawrence River:  
105 the Saguenay, Rimouski, Betsiamites, Aux-Outardes and Manicouagan Rivers. The associated discharge  
106 areas correspond to gently sloping submarine fans (Pinet *et al.*, 2015) with active turbiditic channels  
107 (Normandeau *et al.*, 2017). One of the largest mass-transport complexes is located near a former mouth  
108 of the Betsiamites River (Cauchon-Voyer *et al.*, 2008). Holocene mass-transport deposits are not  
109 consistently present near the mouth of major rivers, suggesting that the actual sedimentary inputs are  
110 not the predominant preconditioning factor for seafloor instability (Normandeau *et al.*, 2015). However,  
111 most of them are located on steep slopes ( $> 5^\circ$ ) bordering the Laurentian Channel, indicating that the  
112 seafloor gradient is an important preconditioning factor for slope instability (Normandeau *et al.*, 2015;  
113 Pinet *et al.*, 2015). If gas charging is considered a preconditioning factor for submarine slope instability  
114 (e.g., Riboulot *et al.*, 2013), no link was clearly established between the presence of free gas and the  
115 mass-transport complexes in the St. Lawrence Estuary (Pinet *et al.*, 2015).

## 116 2.2. Quaternary sedimentation

117 The carbonate platform of the St. Lawrence Estuary is covered by Quaternary sediments with a  
118 maximum thickness of  $\sim 400$  m controlled by the underlying topography of the bedrock (Duchesne *et*  
119 *al.*, 2010). The seismo-stratigraphic sequence of Quaternary sedimentation in the St. Lawrence Estuary,  
120 first established by Syvitski and Praeg (1989), and completed with samples and dating (St-Onge *et al.*,  
121 2008; Duchesne *et al.*, 2010), is composed of five units. Seismic Unit 1 overlies the bedrock. It is  
122 interpreted as ice-contact sediments (Syvitski and Praeg, 1989) when the ice extension was maximum  
123 during the Last Glacial Maximum (LGM: 21000 cal yr BP). Unit 2 corresponds to ice-proximal, coarse-  
124 grained sediments in a glaciomarine environment. Fine-grained, ice-distal sediments characterize Unit  
125 3. Units 2-3 were deposited when the Goldthwait Sea was present in the St. Lawrence Estuary and Gulf  
126 from 13000 to 9000 cal yr BP (Dionne, 2001). Unit 4 marks the transition between glaciomarine and  
127 postglacial sedimentation. It comprises hemipelagic sediments (Duchesne *et al.*, 2010) following the  
128 rerouting of meltwaters of the Laurentide Ice Sheet (LIS) from the St. Lawrence to Hudson Bay after

129 the collapse of the proglacial Lake Agassiz-Ojibway around 8500 cal yr BP (St-Onge *et al.*, 2003).  
 130 Cauchon-Voyer *et al.* (2011) described stratified silty clays with thin layers of sand in Unit 4. Finally,  
 131 Unit 5 differs from Unit 4 by the presence of coarser sediments that were deposited under modern  
 132 oceanographic conditions. Modern sedimentation rates range between 0.74 cm.yr<sup>-1</sup> at the mouth of the  
 133 Lower Estuary to 0.04 cm.yr<sup>-1</sup> in the Gulf, with an exponential decrease (Zhang *et al.*, 2000).



134  
 135 **Fig. 2.** Bathymetric maps of the Betsiamites – Baie Comeau – Rimouski a), of the Forestville – Saguenay  
 136 b) and of the Charlevoix sectors c). The gravity and box cores are respectively represented by red and  
 137 white circles. The black lines correspond to track lines of the acoustic sub-bottom profiler survey.

138 *2.3. Regional seismicity and sediment liquefaction*

139 In addition to the 1663 CE earthquake, four earthquakes with M 5.9 to 6.6 occurred in the CKSZ in  
 140 1860, 1870, 1925 and 1988 CE (Smith, 1962; Lamontagne *et al.*, 2003; Lamontagne *et al.*, 2018) (**Fig.**  
 141 **1**). An average of 200 earthquakes are recorded annually in CKSZ and 50 to 100 in the Lower St.  
 142 Lawrence zone (Lamontagne *et al.*, 2003). They are localized at depths between 5 to 25 km in the  
 143 Precambrian bedrocks (Anglin, 1984). Only a small proportion exceeds M 3.



144 The origin of intraplate earthquakes in Eastern Canada is not clearly identified, but two principal causes  
145 are conceivable: tectonic and glacio-isostatic (Wu, 1998). Most earthquakes are concentrated in the St.  
146 Lawrence Valley and related to a fault inherited from Paleozoic rifting (Adams and Basham, 1989). The  
147 depth of the hypocenters corresponds to the Appalachian thrust fault over the St. Lawrence Platform,  
148 named Logan fault (Anglin, 1984). These evidences support a tectonic origin but only a portion of the  
149 recorded earthquakes can be related to tectonics.

150 Thus, regional studies highlighted a higher frequency of mass movements in the early Holocene (St-  
151 Onge *et al.*, 2004; Cauchon-Voyer *et al.*, 2011) and liquefaction events interpreted as markers of  
152 enhanced seismic activity between 8000 and 1000 cal yr BP (Obermeier *et al.*, 1992). These observations  
153 are consistent with deglaciation in the St. Lawrence region, which resulted in significant glacio-isotactic  
154 adjustment during the early Holocene (Wu, 1998).

155 In addition to tectonic and glacio-isostatic processes, earthquakes can be influenced by fracturing caused  
156 by an asteroid impact in the Charlevoix region about 350 Ma ago (Roy and Du Berger, 1983). The  
157 weakness of the fractured crust coupled with glacio-isostatic rebound could partially explain regional  
158 seismicity and the high earthquake concentration observed by Roy and Du Berger (1983) in the CKSZ.  
159 Seismicity is the main cause of sediment liquefaction (Seed and Idriss, 1967) which can destabilize  
160 submarine slopes and generate submarine landslides (Tuttle and Atkinson, 2010). Indeed, Cauchon-  
161 Voyer *et al.*, (2008, 2011) suggest that the alternation of silty clays and sand layers in Unit 4 of the St.  
162 Lawrence Quaternary sedimentation could influence the permeability of materials and favor an increase  
163 in pore pressure in the case of an earthquake. Consequently, a weak layer in Unit 4 could be generated  
164 during an earthquake, thus promoting the development of slip surface. Based on geotechnical analyses  
165 and numerical simulations, Martin *et al.* (2001) showed that this alternation of silty clays and sand in  
166 Saguenay Fjord sediments implies high liquefaction susceptibility during an earthquake.

167 **3. Data and methods**

168 *3.1. Geophysics*

169 High-resolution swath bathymetry data was collected from 1997 to 2005 between Île-aux-Coudres and  
170 Pointe-des-Monts by the Canadian Hydrographic Service using multibeam echosounder systems  
171 mounted on the Coast Guard Ship *Frederick G. Creed* (before 2005: Kongsberg EM-1000; in 2005:  
172 EM-1002) and launch *Guillemot* (before 2005: EM-3000; in 2005: EM-3002). These surveys provided  
173 a full-bottom coverage below 30 m depths at a resolution of 5 m.

174 In summer 2020, the bathymetric coverage was completed during the SLIDE-2020 cruise on board the  
175 RV *Coriolis II* using a Kongsberg EM-2040 multibeam echosounder system coupled with the Applanix  
176 POS/MV inertial platform. Surveys were conducted in areas where Pinet *et al.* (2015) had previously  
177 mapped mass-transport complexes with the aim to significantly increase the resolution. A new  
178 bathymetric grid with a cell size of 1 m was generated using the Caris Hips & Sips software. Data  
179 acquired during the SLIDE-2020 cruise with the celerimeter *Minos* from *AML oceanographic* were used  
180 to account for the variability of sound velocity in the water column.

181 In addition, high-resolution seismic data were collected (**Fig. 3-4**) using the hull-mounted Edgetech X-  
182 Star 2.1 subsurface profiler. Hence, about 1500 km of seismic profiles were acquired during the SLIDE-  
183 2020 expedition. The source frequency was between 2 and 12 kHz with chirp pulses between 3 and  
184 20 ms. Time-to-depth conversion of the seismic profiles was done using an average sound wave velocity  
185 value of 1500 m.s<sup>-1</sup> corresponding to the velocity in water and the mean value measured on sediment  
186 cores using the Multi Sensor Core Logger. Interpretation of the seismostratigraphic sequence was based  
187 on seismic attributes such as reflections, geometry and amplitude of reflecting horizons detailed by  
188 Cauchon-Voyer *et al.* (2008).

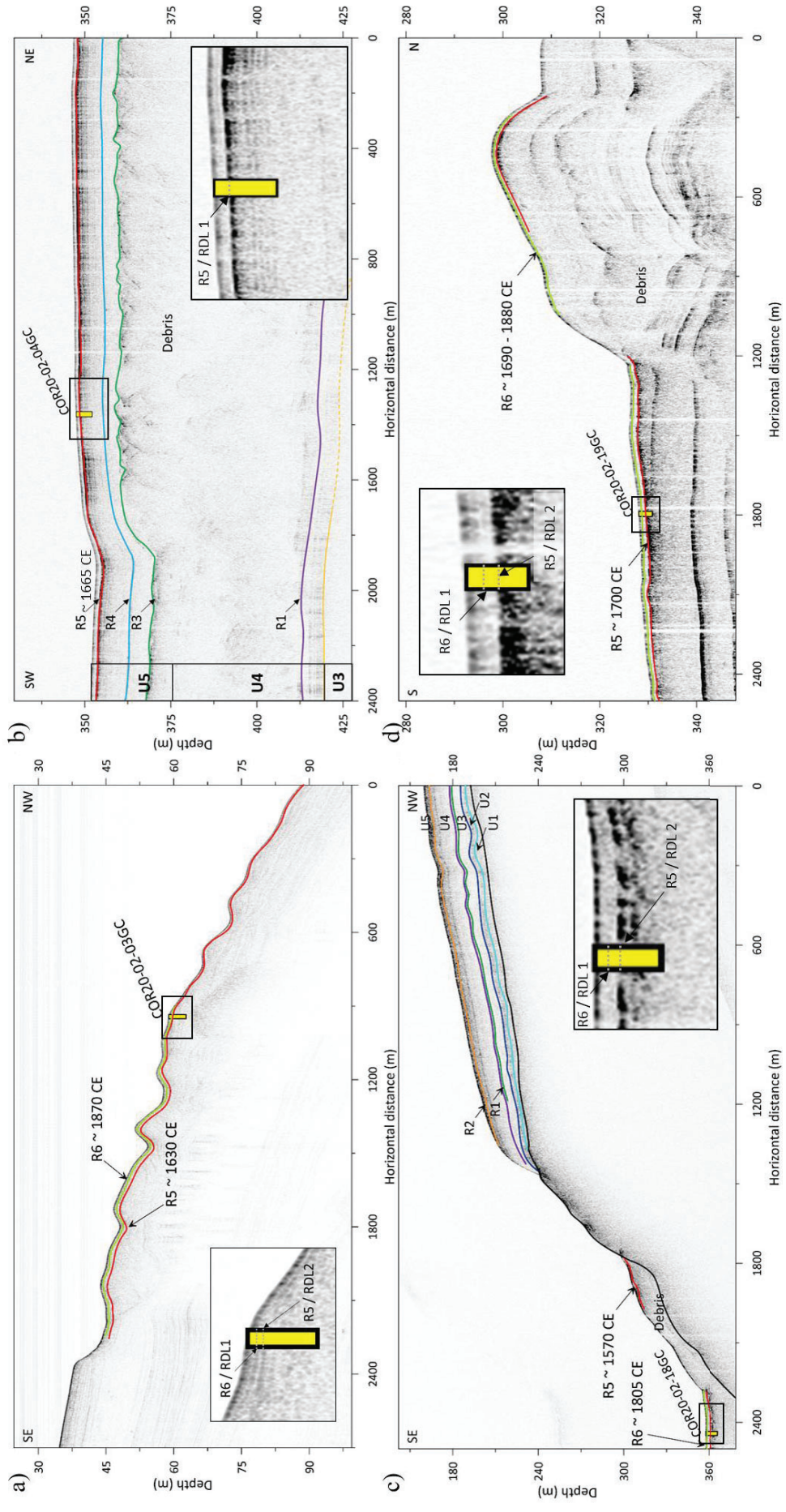
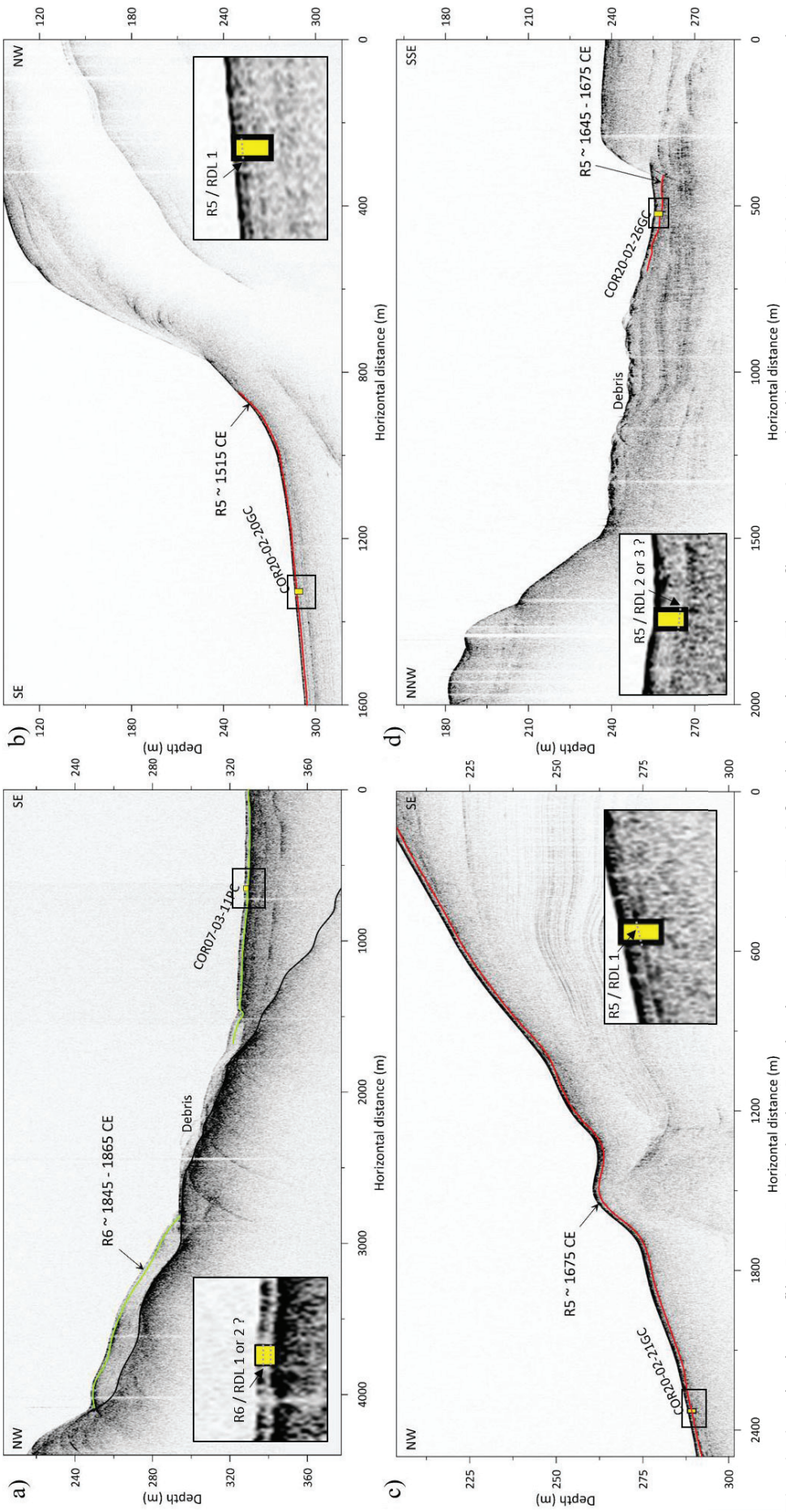


**Fig. 3.** a) Seismic profile RIM\_1T (see Fig. 2 for the locations) on which reflectors R5 and R6 corresponds respectively to turbidites T2 and T1 in core COR20-02-03GC. b) Seismic profile RIM\_1A, transversal to the Betsiamites lobe in the Laurentian Channel. Labels U3 to U5 refer to seismic units and R1 to R5 to seismic horizons described by Cauchon-Voyer *et al.*, (2008). The black square is a close-up view of R5. Reflector R5 correlates with turbidite T1 in the core 20-02-04GC. c) Seismic profile BET\_B\_2T with R5 and R6 reflectors (cf. detailed view in the black square) which correspond to turbidites T3 and T2 in COR20-02-18GC. d) Southern part of seismic profile BET\_D\_2T. Core COR20-02-19GC reaches reflectors R6 and R5 at  $\sim 0.5$  mbsf and  $\sim 1.2$  mbsf, which are respectively interpreted as turbidites T1 and T2. See supplementary data for uninterpreted seismic profiles.



196 **Fig. 4.** a) Seismic profile BET\_D\_3T in the Betsiamites area (see Fig. 2 for the locations). The reflector R6 reached by core COR07-03-1IPC, corresponds to  
 197 turbidite T1 or T2 dated around 1845-1865 CE. b) Seismic profile FOR\_A\_1T. Turbidite T1 in core COR20-02-20GC corresponds to R5. c) Seismic profile  
 198 ESC\_BCD\_1T. Reflector R5 (cf. detailed view in the black square) correlates with turbidite T1 sampled in core COR20-02-21GC. See supplementary data for  
 199 the uninterpreted seismic profiles. d) The seismic profile SAG\_H\_1T with reflector R5 at the toe of a mass transport deposit. It corresponds to turbidites T2 or  
 200 T3 observed in core COR20-02-26GC. See supplementary data for the uninterpreted seismic profiles.

### 202 3.2. Core sampling

203 During the SLIDE-2020 expedition, cores were recovered over a distance of more than 200 km along  
204 the St. Lawrence Estuary, at water depths between 34 and 354 m (**Fig. 2**). The cores were collected in  
205 the CKBSL seismic zone. All thirteen gravity cores and four box cores recovered during SLIDE-2020  
206 are used in this study (**Table 1** and **Fig. 2**). Box cores were subsampled with push cores connected to a  
207 pump to avoid compaction of sediment. Unlike gravity cores, they do not disturb the sediment/water  
208 interface, which allows for correlation of the gravity and box cores, as well as the use of  $^{210}\text{Pb}$  dating on  
209 the box cores. The gravity corer used had a maximum length of 6 m. This study also used two piston  
210 cores of 2.5 m and 4.1 m long that were recovered during the COR07-03 expedition (RV *Coriolis II*,  
211 Cauchon-Voyer *et al.*, 2007).

212 The core sites are located in the distal part of the mass-transport deposit in order to sample the finest  
213 part of the submarine landslide allowing to date the hemipelagic sediment above and below the RDLs.  
214 The targeted RDLs are theoretically not affected by local sedimentary processes because they were  
215 selected neither at the mouth of active rivers, nor at the end of active turbidity current channels (e.g.,  
216 Normandeau *et al.*, 2017), or in pockmark-rich areas described by Pinet *et al.* (2015). However, due to  
217 the estuarine context, regional sedimentary processes such as hyperpycnal flows could occur in the St.  
218 Lawrence Estuary.

### 219 3.3. Sedimentological analyses

220 Wet bulk density, low-field volumetric magnetic susceptibility ( $k$ ) and P-Wave velocity were measured  
221 using the GEOTECK MSCL (Multi Sensor Core Logger) at ISMER (St-Onge *et al.*, 2007; **Fig. 5-6**).  
222 Measurements were performed at intervals of 1 cm on whole sections of gravity cores and 0.5 cm on  
223 whole sections subsampled from the box cores.

224 After splitting the cores, archived halves were photographed and described (texture, color, lithology,  
225 structures and bioturbation). Subsequent digital X-ray images were then acquired with the GEOTECK  
226 XCT scanner. This non-destructive measurement allows to visualize the sedimentary structures. The  
227 denser materials that compose the RDLs appear as light gray on the X-ray images. On split cores, bulk

228 magnetic susceptibility ( $k$ ) was measured with a point source sensor, while  $L^*$ ,  $a^*$  and  $b^*$  color  
229 parameters were determined using the Minolta CM-2600d spectrophotometer at 1 cm intervals (**Fig. 5-**  
230 **6**). Because  $k$  increases slightly with increasing grain size, this parameter is used to identify RDLs  
231 following the method presented by St-Onge *et al.* (2007). Grain-size analysis (1 to 2 000  $\mu\text{m}$ ) was  
232 performed using the Master Sizer 3000 (Malvern) laser grain size analyzer with sampling intervals of 1  
233 to 2 cm in each RDL and 5 to 20 cm for the background sedimentation. Prior to their analysis, the  
234 samples were diluted in a solution composed of distilled water and hexametaphosphate and stirred for  
235 24 h to deflocculate clay particles.

236 The geochemical composition was measured on archive halves using the non-destructive Olympus  
237 Innov-X Delta X-Ray Fluorescence (XRF) scanner in line with the MSCL. The spacing of XRF  
238 measurements was similar to that of the other measurements previously mentioned. In this study, the  
239 Ca/Fe ratio (biogenic/detrital proxy) and the Rb/Zr ratio (grain size proxy) were used as criteria to  
240 identify RDL (Croudace *et al.*, 2006) and to help distinguish the top of RDLs from hemipelagic  
241 sedimentation (**Fig. 5-6**). RDLs are numbered between 1 for the youngest and 7 for the oldest and are  
242 site-specific. As such, the RDL numbers do not refer to the synchronicity of the deposits.

### 243 3.4. Dating

244 Radiocarbon dating was performed on 45 samples of shells or organic matter that were sampled close  
245 to the bases of RDL in the hemipelagic sediments (**Table 2**). After pre-treatment and graphitization at  
246 the *Centre d'études nordiques* at Université Laval (Québec City), they were measured at the Keck-  
247 Carbon Cycle AMS facility at the University of California Irvine (USA). To obtain accurate RDL  
248 chronology, the  $^{14}\text{C}$  ages of hemipelagic samples were calibrated using the Calib 8.2 software (Stuiver  
249 and Reimer, 1993) and the Marine20 curve (Heaton *et al.*, 2020). To consider the local offset from the  
250 global ocean reservoir ( $\Delta\text{R}$ ), two reservoir ages from McNeely *et al.* (2006) were used. These reservoir  
251 ages are closest to the study area with one at Matane of  $\Delta\text{R} = 77 \pm 60$   $^{14}\text{C}$  yr and one at Pointe John of  
252  $\Delta\text{R} = -13 \pm 70$   $^{14}\text{C}$  yr. They were averaged to have a final reservoir age of  $\Delta\text{R} = 39 \pm 63$   $^{14}\text{C}$  yr for shell

253 samples. Finally, the radiocarbon ages were converted to calendar ages (CE) for comparison with  
 254 historical earthquakes (**Table 2**).

255 **Table 2.** Radiocarbon analyses from cores recovered in the St. Lawrence Estuary (Québec).

Core	Lab. num.	Depth (cm)	Sample type	<sup>14</sup> C age (BP)	ΔR	Calibrated age (yr BP) ± 1σ	Calibrated age (CE) ± 1σ
<i>COR07-03-13PC</i>	ULA-9628	10.00	Organic matter	255 ± 15	-	300 ± 5	1650 ± 5
<i>COR20-02-03GC</i>	ULA-9787	8.00	Shell	Modern	39 ± 63	-55 ± 5	2005 ± 5
	ULA-9788	89.50	Shell	765 ± 15	39 ± 63	180 ± 95	1770 ± 95
	ULA-9789	99.50	Shell	780 ± 20	39 ± 63	195 ± 100	1755 ± 100
	ULA-9790	135.50	Shell	920 ± 15	39 ± 63	345 ± 85	1605 ± 85
	ULA-9791	356.75	Shell	2020 ± 20	39 ± 63	1380 ± 90	570 ± 90
<i>COR20-02-04GC</i>	ULA-9645	47.00	Shell	745 ± 15	39 ± 63	165 ± 95	1785 ± 95
	ULA-9642	92.50	Shell	965 ± 15	39 ± 63	380 ± 80	1570 ± 80
	ULA-9644	109.50	Shell	1095 ± 15	39 ± 63	495 ± 80	1455 ± 80
<i>COR20-02-13GC</i>	ULA-9652	17.50	Shell	1190 ± 15	39 ± 63	570 ± 50	1380 ± 50
	ULA-9653	19.50	Shell	1210 ± 15	39 ± 63	585 ± 70	1365 ± 70
	ULA-9647	84.75	Shell	2915 ± 15	39 ± 63	2465 ± 115	-515 ± 115
	ULA-9648	161.50	Shell	4875 ± 15	39 ± 63	4920 ± 110	-2970 ± 110
<i>COR20-02-14GC</i>	ULA-9792	9.25	Shell	675 ± 20	39 ± 63	110 ± 80	1840 ± 80
	ULA-9793	46.0.	Shell	1640 ± 15	39 ± 63	995 ± 95	955 ± 95
	ULA-9794	65.00	Shell	2020 ± 15	39 ± 63	1380 ± 175	570 ± 175
	ULA-9816	71.50	Shell	2125 ± 15	39 ± 63	1490 ± 195	465 ± 195
	ULA-9817	97.50	Shell	2780 ± 15	39 ± 63	2280 ± 220	-330 ± 220
<i>COR20-02-17GC</i>	ULA-9818	73.50	Shell	1655 ± 20	39 ± 63	1010 ± 95	940 ± 95
	ULA-9819	198.75	Shell	3285 ± 20	39 ± 63	2895 ± 105	-945 ± 105
	ULA-9820	259.50	Shell	4590 ± 15	39 ± 63	4565 ± 120	-2615 ± 120
<i>COR20-02-18GC</i>	ULA-9654	80.25	Shell	1180 ± 15	39 ± 63	565 ± 70	1385 ± 70
	ULA-9682	204.50	Shell	3690 ± 20	39 ± 63	3395 ± 105	-1445 ± 105
	ULA-9620	213.25	Wood	3395 ± 15	-	3030 ± 80	-1135 ± 80
	ULA-9655	331.50	Shell	8485 ± 20	39 ± 63	8835 ± 125	-6885 ± 125
<i>COR20-02-19GC</i>	ULA-925	14.00	Alga	Modern	-	-45 ± 5	1995 ± 5
	ULA-9646	201.50	Shell	2460 ± 15	39 ± 63	1885 ± 210	65 ± 210
<i>COR20-02-20GC</i>	ULA-9650	40.00	Shell	790 ± 20	39 ± 63	205 ± 100	1745 ± 100
	ULA-9669	204.50	Shell	2255 ± 20	39 ± 63	1635 ± 100	315 ± 100
	ULA-9670	423.50	Shell	3915 ± 15	39 ± 63	3670 ± 110	-1720 ± 110
<i>COR20-02-21GC</i>	ULA-9671	96.00	Shell	920 ± 15	39 ± 63	345 ± 85	1605 ± 85
	ULA-9672	178.50	Shell	2175 ± 15	39 ± 63	1545 ± 105	405 ± 105
<i>COR20-02-50GC</i>	ULA-9784	46.50	Wood	Modern	-	-40 ± 5	1990 ± 5

257 To construct the best-fit age models, the R software package Bacon 2.3 (Blaauw and Christen, 2011)  
258 was used. It considers Bayesian statistics with a normal distribution. Both standard deviations of  $1 \sigma$   
259 (probability of 0.95) and  $2 \sigma$  (probability of 0.68) were used in calculations (**Fig. 7**). In these  
260 calculations, turbidite erosion was assumed negligible because it was not possible to quantify basal  
261 erosion.

262 Sedimentation rates were derived from  $^{210}\text{Pb}$  measurements on sediments from 4 box cores (**Table 3** and  
263 **Fig. 8**). The cores were sampled at intervals ranging from 1 to 5 cm and freeze-dried, then ground to a  
264 fine, homogenous powder. The  $^{210}\text{Pb}$  activity was measured using a GMX50-S gamma counter from  
265 Ortec and GX7020 counter from Canberra. Considering the constant flux and constant rate model  
266 (Appleby and Oldfield, 1978), the sedimentation rates ( $\text{cm.yr}^{-1}$ ) were derived from the slope of  
267  $\text{Ln}(^{210}\text{Pb}_{\text{excess}})$  in the region of radioactive decay (**Fig. 8**). The ages of turbidites were then calculated by  
268 extrapolating a constant sedimentation rate down to the hemipelagic depth of turbidites. Sediment  
269 compaction is neglected because the density curve of hemipelagic sedimentation appears constant with  
270 depth (**Fig. 8**).

## 271 **4. Results**

### 272 *4.1. Facies identification*

273 The four cores presented in **Fig. 5** and **Fig. 6** show the sedimentary facies observed on analyzed cores.  
274 They were selected to best illustrate the characteristics of the different types of RDLs. An exhaustive  
275 list of all the sediment cores is presented in the supplementary data. The results of core analysis  
276 identified two main facies: hemipelagites and RDLs (**Fig. 5-6**). Hemipelagites are consistent with  
277 normal “background”, hemipelagic sedimentation while RDLs are a result of almost instantaneous  
278 deposition. Hemipelagites consist of homogenous gray-colored silts (Munsell value 5YR 5/1). The gray  
279 tone varies with the intensity of bioturbation from dark gray (5YR 4/1) to very dark gray (5YR 3/1). The  
280 hemipelagites are composed of 10 – 20 % clay ( $< 2 \mu\text{m}$ ), 65-75 % silt (2-63  $\mu\text{m}$ ) and 10 – 20 % sand  
281 (63 $\mu\text{m}$  - 2 mm). Their gamma density values are constant with depth and oscillate between 1.4 and  
282 1.6  $\text{g.cm}^{-3}$ . On X-ray images, hemipelagites appear in homogenous black gray and their values of

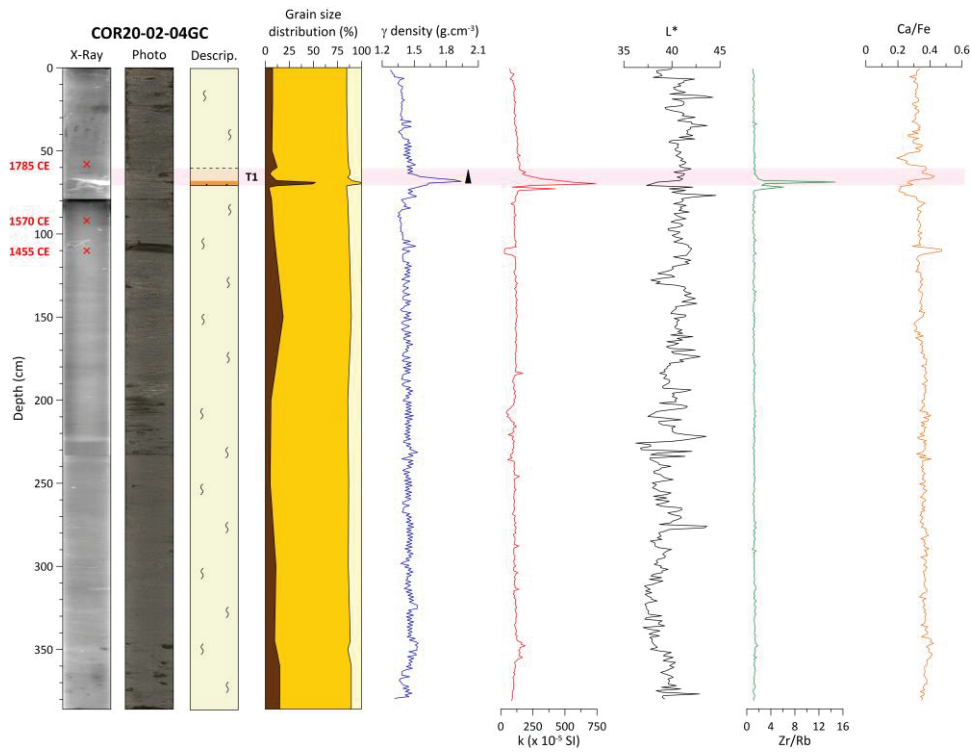


283 magnetic susceptibility are relatively low ( $\sim 125 \cdot 10^{-5}$  SI) compared to RDLs ( $\sim 500 \cdot 10^{-5}$  to  $750 \cdot 10^{-5}$  SI).  
284 Overall, hemipelagites have the same properties across the St. Lawrence Estuary, though they are  
285 generally coarser in the Middle Estuary with 10% clay, 80% silt and 10% sand (e.g., COR20-02-50GC).  
286 Likewise, the thickness of hemipelagites is between 10 – 20 cm in the Lower Estuary (e.g., COR20-02-  
287 50GC) and higher than 50 cm in the Middle Estuary (e.g., COR20-02-04GC).

288 On X-Ray images, light gray layers intersect the hemipelagic sedimentation. These layers correspond to  
289 RDL facies. Their physical properties, detailed below, contrast clearly with background sedimentation  
290 and their bases are mainly sharp, while their upper contacts are gradational. The internal structure and  
291 grain size distribution vary between RDLs, such that four groups can be distinguished: turbidites (T),  
292 debrites (D), hyperpycnites (H) and slump (S).

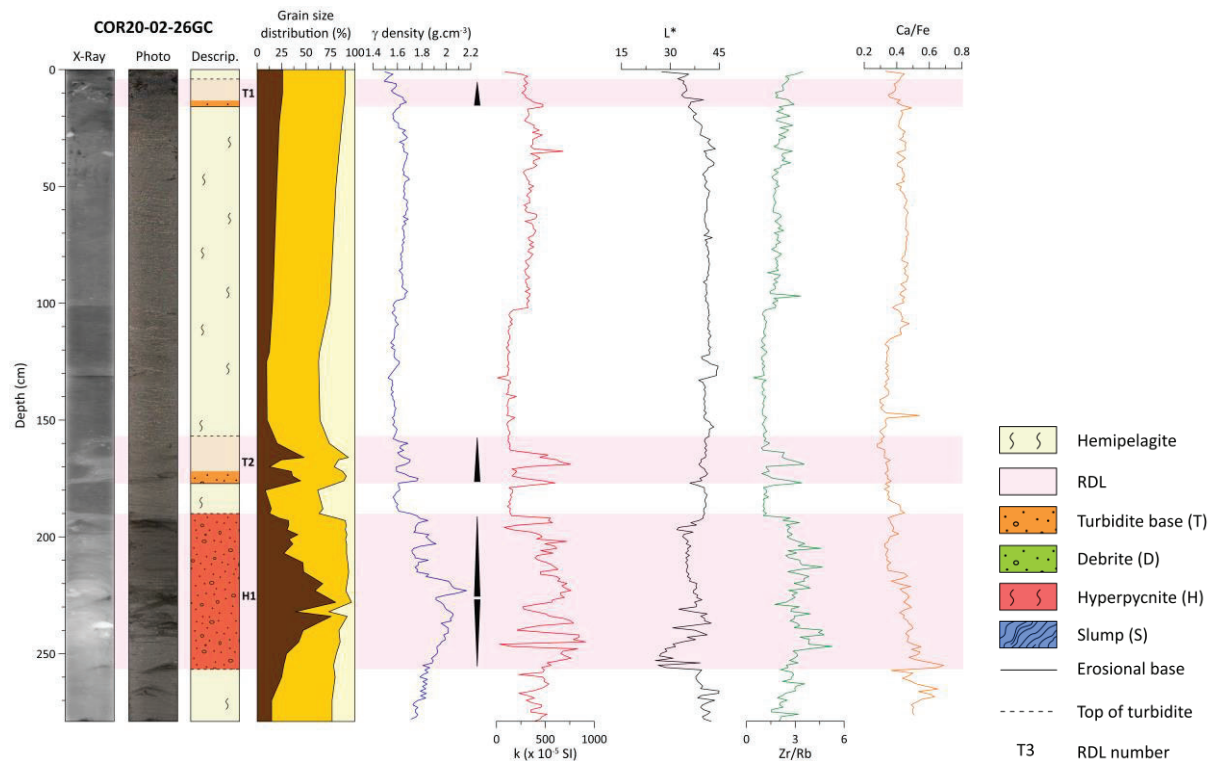
293 In the 15 cores, 43 turbidites (T) were identified (see supplementary data). Their thickness varies  
294 between  $\sim 3$  and 73.5 cm with a mean value of 18.5 cm (**Table 4**). The bases are sharp and the grain size  
295 analyses reveal a normal grading typical of the Bouma-type turbidite (Bouma, 1962). Indeed, turbidites  
296 are characterized by a sandy base (fine to coarse sand) with sometimes gravels or rock fragments  
297 ( $< 2$  mm) as in turbidite T1 in core COR20-02-21GC. The coarser material at the base of the turbidite  
298 layers is associated with high values of density and magnetic susceptibility, contrasting sharply with the  
299 overlying and underlying hemipelagic sediments. In core COR20-02-04GC (**Fig. 5**), turbidite T1  
300 presents a maximum density of  $1.93 \text{ g.cm}^3$  and a magnetic susceptibility of  $744 \cdot 10^{-5}$  SI, which both  
301 contrast with values of  $1.45 \text{ g.cm}^3$ , and  $144 \cdot 10^{-5}$  SI in hemipelagic sediments. The coarse base of this  
302 turbidite layer likely comprises heavy minerals such as magnetite (e.g., Goldfinger *et al.*, 2007; Jaegle,  
303 2015) and is darker ( $L^* = 37.5$ ) compared to the under- and overlying background sediments ( $L^* =$   
304  $40.5$ ), suggesting that this parameter could be used to discriminate the base of turbidites. Furthermore,  
305 the two chosen geochemical ratios in core COR20-02-04GC are relatively constant in the hemipelagites  
306 ( $\text{Zr/Rb} = 1.22$  and  $\text{Ca/Fe} = 0.34$ ), but follow the grain size evolution of the turbidites with the highest  
307 values at the base ( $\text{Zr/Rb} = 14.75$  and  $\text{Ca/Fe} = 0.43$ ) gradually decreasing toward the top. These  
308 geochemical signatures, sensitive to grain size, can be used in addition to the previous parameters to  
309 accurately identify the base and top of turbidites.

310 a)



311

312 b)



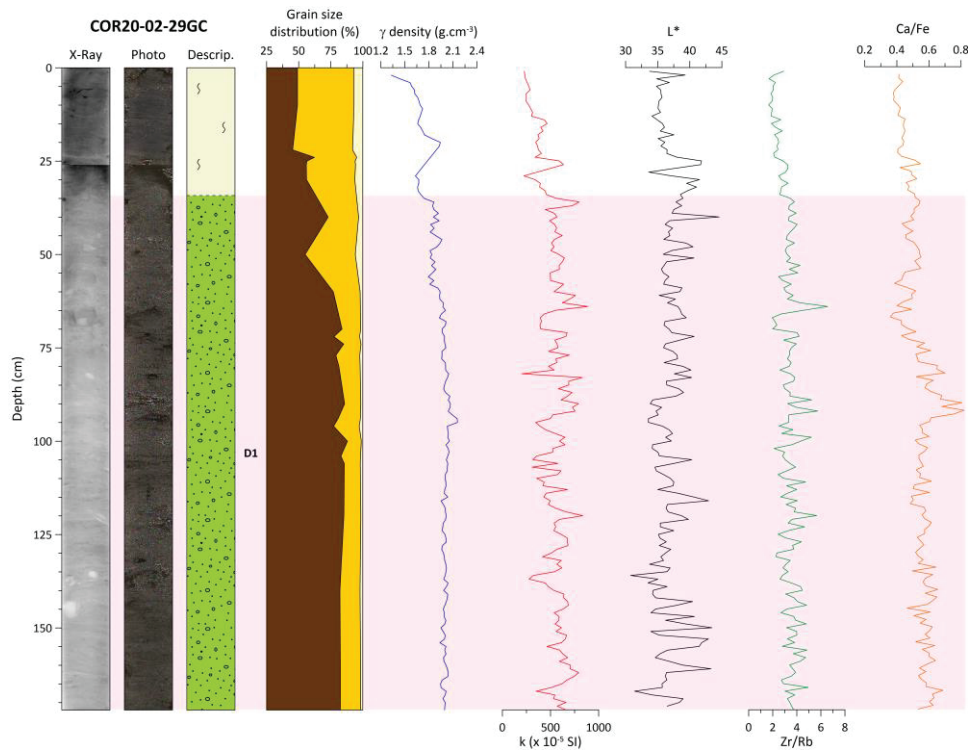
313

314 **Fig. 5.** Results of the sedimentological analyses carried out on cores a) COR20-02-04GC and b) COR20-

315 02-26GC. From left to right: X-ray image, digital photography, sedimentological description,  $\gamma$ -density,

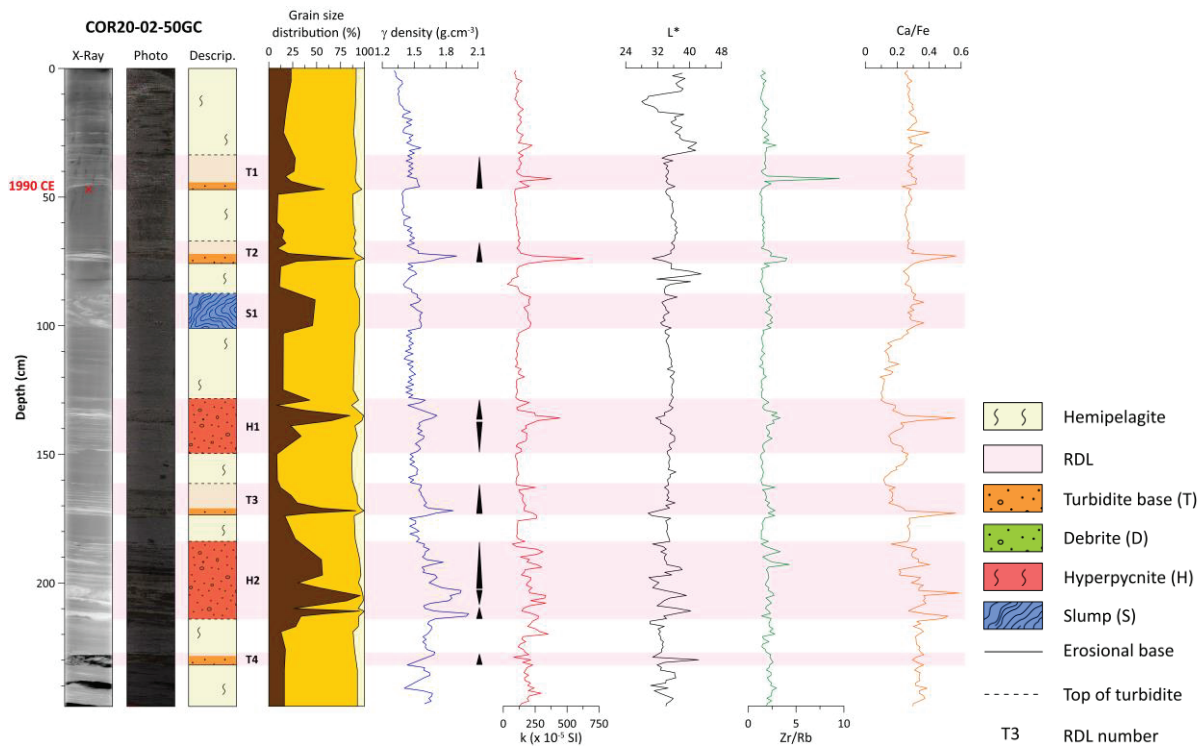
316 magnetic susceptibility  $k$ , lightness  $L^*$ , Zr/Rb and Ca/Fe.

317 a)



318

319 b)



320

321 **Fig. 6.** Results of the sedimentological analyses carried out on cores a) COR20-02-29GC and b) COR20-

322 02-50GC. From left to right: X-ray image, digital photography, sedimentological description,  $\gamma$ -density,

323 magnetic susceptibility  $k$ , lightness  $L^*$ , Zr/Rb and Ca/Fe.

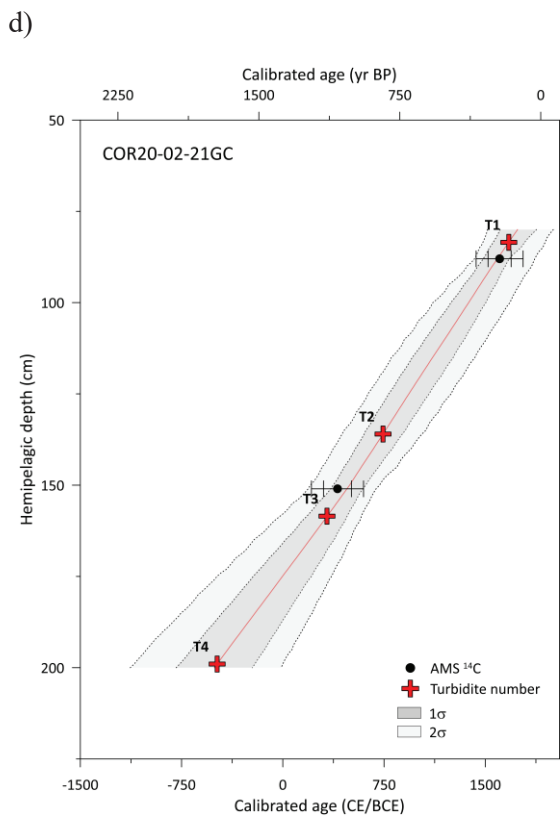
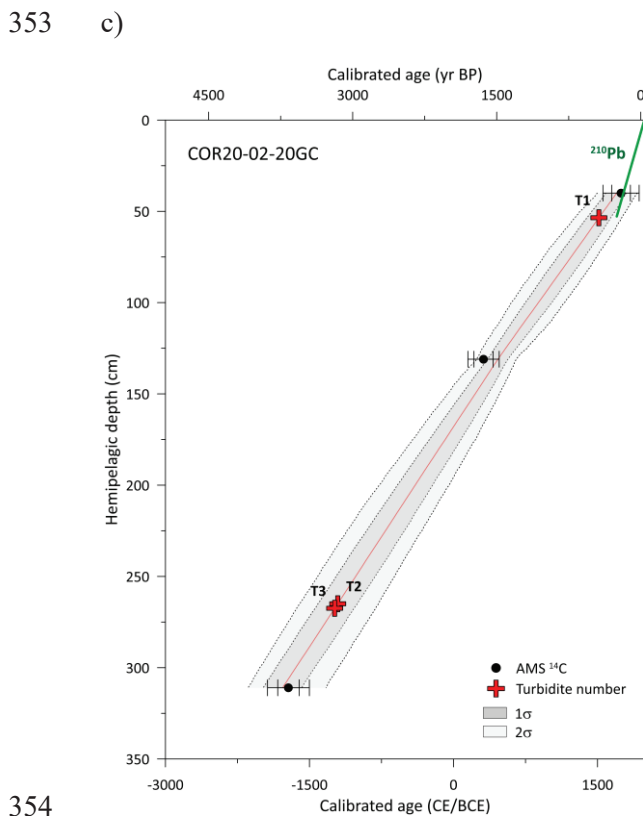
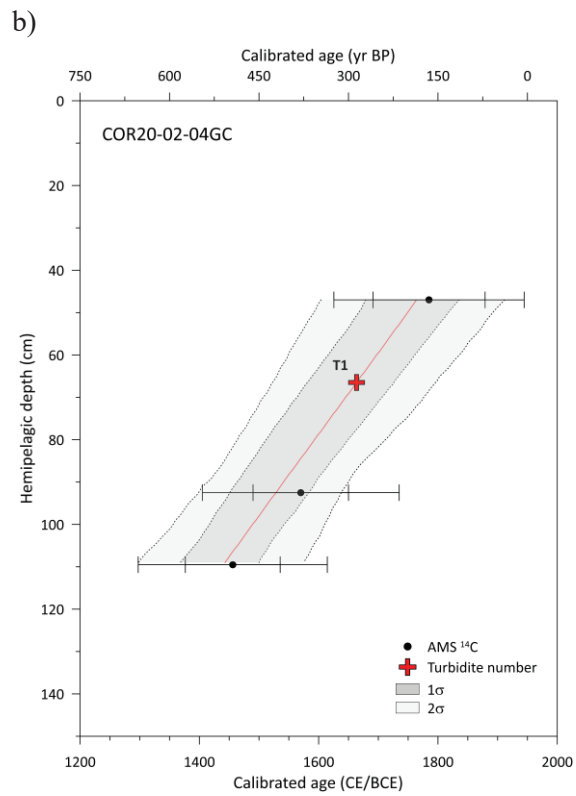
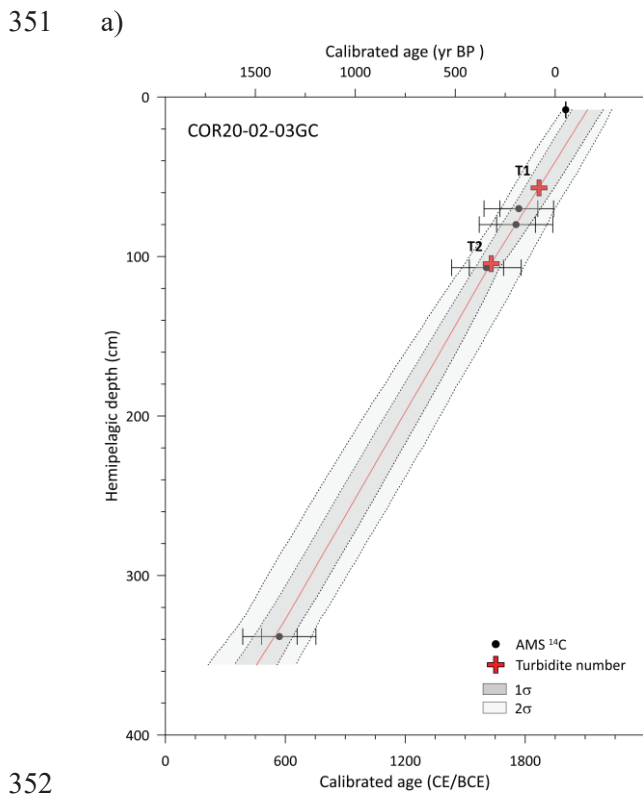
324 Debrites (D) produced by debris flows constitute the second type of RDL identified in sediment cores.  
325 Only four debrites are identified in four cores. These deposits are more proximal to the source of  
326 submarine landslides than turbidites. The debrites include rock fragments up to ~10 cm in length,  
327 observable on XCT images (**Fig. 6**). As shown in D1 of core COR20-02-29GC, these rock fragments  
328 vary in nature, size, angularity and orientation in a sandy-silty matrix composed of 75% sand, 20% silt  
329 and 5% clay ( $D_{50} \sim 150 \mu\text{m}$ ). Thus, cores containing debrite layers are relatively short because the corer  
330 could not fully penetrate these deposits, unlike turbidites. Density and magnetic susceptibility are high  
331 with average values of respectively  $1.95 \text{ g/cm}^3$  and  $560.10^{-5} \text{ SI}$  in core COR20-02-29GC. In addition,  
332 contrary to turbidites, the debrites are massive and chaotic with no observable grading. The debrite in  
333 core COR07-03-11PC (D1) (see supplementary data) is composed of a block of terrestrial organic  
334 material. Larger rock fragments are observed at the base of the debrite layer.

335 The RDLs characterized by reverse grading at the base followed by normal grading are interpreted as  
336 hyperpycnites (H) resulting from a hyperpycnal flow (Mulder *et al.*, 2003; St-Onge *et al.*, 2004).  
337 Hyperpycnites were observed in core COR20-02-26GC (**Fig. 5**) recovered near the mouth of the  
338 Saguenay Fjord (~5 km). The reverse grading at its base (256.5 – 226 cm) corresponds to the rising limb  
339 of the flood. Above 226 cm, the normal grading (226 – 190 cm) reflects the falling limb. Two  
340 hyperpycnites are also found in core COR20-02-50GC (**Fig. 6**) sampled in the La Malbaie area.

341 A fourth type of RDL is characterized by the presence of a slump deposit (S) (**Fig. 6**). This deposit was  
342 found only at 100 cm in core COR20-02-50GC. This is a 13.5-cm thick layer of silty-sand inducing  
343 peaks in density, magnetic susceptibility and Zr/Rb. The grains are not sorted and strong internal  
344 deformation is recognizable on the X-ray images. In summary, 43 of the RDLs are turbidites, four are  
345 debrites, three are hyperpycnites and one is a slump, highlighting the higher proportion of turbidites.

#### 346 4.2. Age of the RDLs

347 The radiocarbon and  $^{210}\text{Pb}$  results provided dating of 51 RDLs from 15 different cores (**Table 4**). The  
348 ages are between around 5035 cal yr BP and ~1991 CE. Only four age models are presented here (**Fig.**  
349 **7**), the others are available in the supplementary data. In the next sections, the age of the RDLs are  
350 described for each area.



356 **Fig. 7.** Age models for cores COR20-02-03GC a), COR20-02-04GC b), COR20-02-20GC c) and  
 357 COR20-02-21GC d). The hemipelagic depth, i.e., depth excluding RDLs, is plotted as a function of  
 calibrated ages (BP and CE/BCE). The black circles correspond to the dated samples and the red crosses

358 to the turbidites. The age probability of  $2\sigma$  and that of  $1\sigma$ , are respectively shown in light and medium  
359 gray tone.

#### 360 *Baie-Comeau*

361 In the Baie-Comeau sector, turbidites T1, T2, T3, T4 and T5 in core COR20-02-13GC were deposited  
362 respectively ~1145 CE, 520 CE, 4525 cal yr BP, 4905 cal yr BP and 4940 cal yr BP. In COR20-02-  
363 14GC, four turbidites were deposited more recently around 1580 CE for the uppermost turbidite T1 and  
364 1085 CE, 635 CE and 3270 cal yr BP for turbidites T2, T3 and T4.

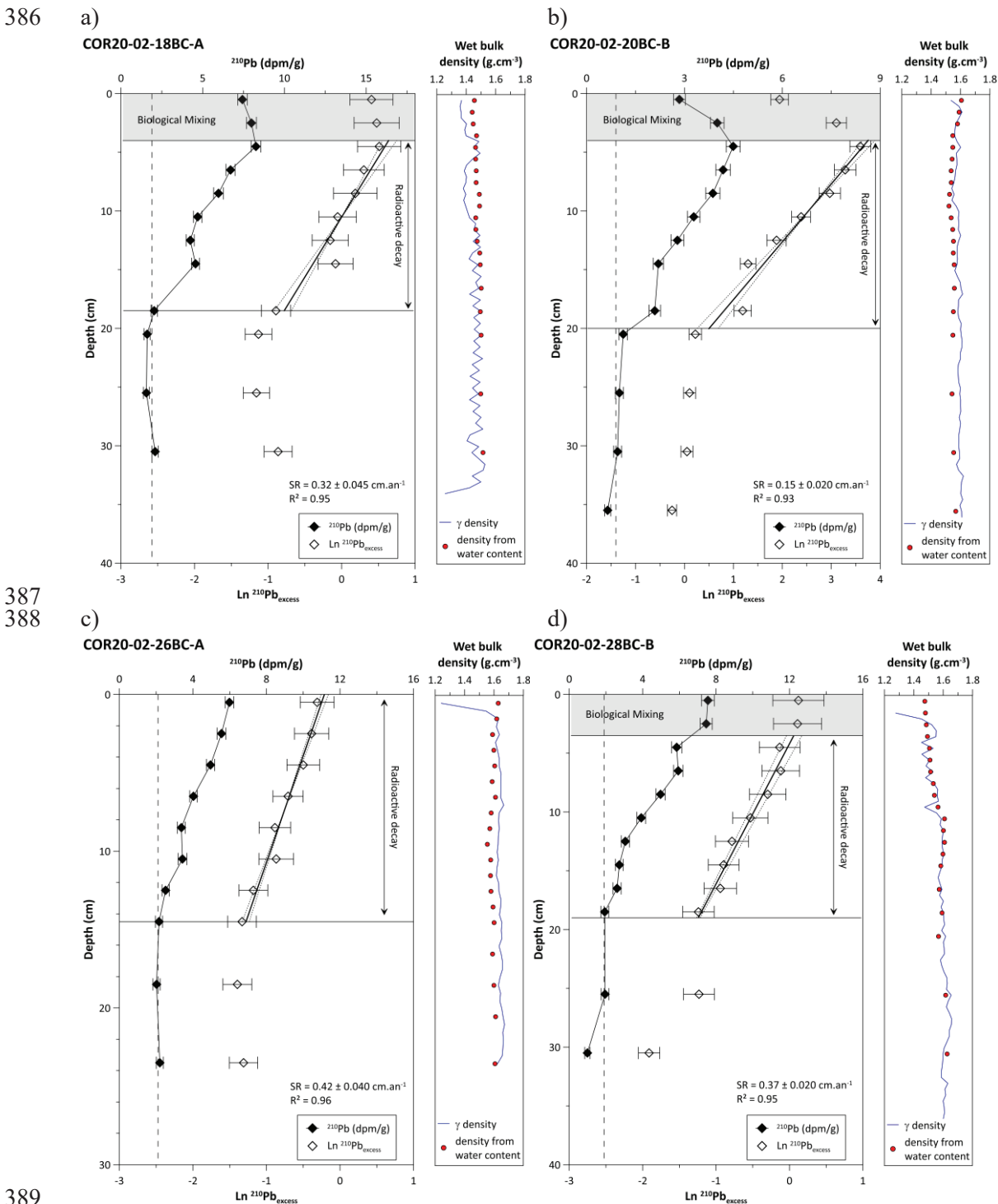
#### 365 *Betsiamites-Rimouski*

366 Further west, in the Betsiamites area, the most recent turbidites (T1) in cores COR20-02-17GC and  
367 COR20-02-18GC are both dated ~ 1640 – 1680 CE while turbidite T2 in core COR20-02-17GC is dated  
368 around 1560 CE. The age of the oldest turbidites is estimated at 5035 cal yr BP (T7) and 4830 cal yr BP  
369 (T6). Sedimentation rates calculated from the box core COR20-02-18BC-A provide respective ages of  
370 1905 CE and 1805 CE for turbidites T1 and T2. In core COR07-03-13PC recovered in the submarine  
371 landslide scar of the Betsiamites area, debrite D1 is estimated to be ~ 1650 CE based on dating of an  
372 intact block of terrestrial material. Turbidites T1 in cores COR20-02-04GC and COR20-02-19GC are  
373 dated to 1665 CE and 1690 CE respectively. Turbidite T2 in core COR20-02-19GC is older with an age  
374 of 1115 CE. The  $^{210}\text{Pb}$ -derived sedimentation rate of  $0.32\text{ cm.yr}^{-1}$  in box core COR20-02-18BC-A yields  
375 more recent ages of 1880 CE and 1700 CE for T1 and T2 respectively. When considered for the nearby  
376 core COR07-03-11PC, this sedimentation rate gives an age of 1865 CE for turbidite T1 and 1845 CE  
377 for T2. On the other side of the St. Lawrence Estuary, near of the city of Rimouski, turbidite T1 is dated  
378 at 1870 CE and T2 at 1630 CE.

#### 379 *Forestville*

380 In core COR20-02-20GC, collected in the Forestville area, turbidite T1 at a depth of 53.5 cm is dated at  
381 1515 CE. Based on a  $^{210}\text{Pb}$ -derived sedimentation rate of  $0.15\text{ cm.yr}^{-1}$  calculated from the associated  
382 box core COR20-02-20BC-B, turbidite T1 dates back to 1665 CE. The older turbidites T2 and T3 are  
383 dated respectively to 3155 cal yr BP and 3190 cal yr BP. In core COR20-02-21GC, recovered near a

384 submarine landslide, turbidite T1 is observed at 83.5 cm depth and dated at 1675 CE. Turbidites T2, T3  
 385 and T4 in core COR20-02-21GC have older ages of 745 CE, 325 CE and 2435 cal yr BP.



389 **Fig. 8.** Sedimentation rates (SR) calculated with the <sup>210</sup>Pb activity in cores COR20-02-18BC-A (SR =  
 390 0.32 cm.yr<sup>-1</sup>, a), COR20-02-20BC-B (SR = 0.15 cm.yr<sup>-1</sup>, b), COR20-02-26BC-A (SR = 0.42 cm.yr<sup>-1</sup>, c)  
 391 and COR20-02-28BC-B (SR = 0.37 cm.yr<sup>-1</sup>, d). SR are calculated from the slope of Ln (<sup>210</sup>Pb<sub>excess</sub>) in  
 392 the radioactive zone by excluding the biological mixing.  
 393

394 *Saguenay*

395 In the Saguenay area, the RDLs could not be dated by  $^{14}\text{C}$  due to the absence of datable material.  
 396 However, two sedimentation rates of  $0.42 \text{ cm.yr}^{-1}$  and  $0.37 \text{ cm.yr}^{-1}$  were calculated from the  $^{210}\text{Pb}$   
 397 measurements in box cores COR20-02-26BC-A and COR20-02-28BC-B, respectively. The turbidite T1  
 398 found at 4 cm depth in core COR20-02-26GC can thus be dated to 2010 CE, whereas turbidite T2 at  
 399 145 cm is dated at 1675 CE and the hyperpycnite H1 (158 cm) at 1645 CE. The debrite D1 identified in  
 400 COR20-02-28GC-3 was dated at 1885 CE using the  $^{210}\text{Pb}$  derived sedimentation rate of  $0.37 \text{ cm.yr}^{-1}$  in  
 401 box core COR20-02-28BC. Close to this coring site ( $\sim 2.5 \text{ km}$ ), at the same water depth, core COR20-  
 402 02-29GC sampled the deposit linked to another submarine landslide. By using the sedimentation rate of  
 403 box core COR20-02-28GC-3, the debrite D1 at 34 cm depth was dated at 1930 CE.

404 **Table 3.** Sedimentation rates calculated and used in this study.

Box cores #	Date of sample (mm-dd-yyyy)	Sedimentation rate ( $\text{cm.yr}^{-1}$ )	Error $\pm 1 \sigma$ ( $\text{cm.yr}^{-1}$ )
COR20-02-18BC-A	07-22-2020	0.32	0.045
COR20-02-20BC-B	07-23-2020	0.15	0.020
COR20-02-26BC-A	07-24-2020	0.42	0.040
COR20-02-28BC-B	07-24-2020	0.37	0.020

405 *La Malbaie*

406 In core COR20-02-50G from the Malbaie area, only one wood fragment could be sampled and dated at  
 407 1990 CE. As the hemipelagic sediments are close to the base of turbidite T1 from that core ( $\sim 0.5 \text{ cm}$ ),  
 408 we can consider an age of 1990 CE for T1. With seven RDLs preserved in a relatively short core  
 409 ( $\sim 2.28 \text{ m}$ ), core COR20-02-50GC presents the highest frequency of RDLs of all the studied cores.



410 **Table 4.** Age  $^{14}\text{C}$  (CE/BCE) of turbidites, hyperpycnites and debrites identified in the 15 cores used in  
 411 this study (see supplementary data for all age models and sedimentological analyses of all cores).

Layer	Total depth (cm)	Hemipelagic depth (cm)	Thickness (cm)	Type of deposit	Estimated $^{14}\text{C}$ age (yr BP), or (CE) when reported	Error $\pm 1 \sigma$	Estimated age $^{210}\text{Pb}$ (CE)	Error $\pm 1 \sigma$
<b>Baie-Comeau</b>								
<i>COR20-02-13GC</i>								
RDL1	23	23	13	Turbidite	1145 CE	110		
RDL2	50.5	37.5	18.5	Turbidite	520 CE	260		
RDL3	181	149.5	11	Turbidite	4525	645		
RDL4	210.5	168	55.5	Turbidite	4905	640		
RDL5	268	170	33	Turbidite	4940	660		
<i>COR20-02-14GC</i>								
RDL1	15	15	15	Turbidite	1580 CE	135		
RDL2	43	28	3	Turbidite	1085 CE	95		
RDL3	64	46	3	Turbidite	635 CE	315		
RDL4	153.5	132.5	8.5	Turbidite	3270	320		
<b>Betsiamites</b>								
<i>COR20-02-17GC</i>								
RDL1	14	14	4.5	Turbidite	1680 CE	180		
RDL2	25.5	21	12.5	Turbidite	1560 CE	180		
RDL3	104	87	7	Turbidite	195 CE	220		
RDL4	124	100	11	Turbidite	2075	235		
RDL5	173	138	21.5	Turbidite	3020	175		
RDL6	241.5	185	15	Turbidite	4540	395		
RDL7	279	207.5	18	Turbidite	5035	430		
<i>COR20-02-18GC</i>								
RDL1	37.5	37.5	13.5	Turbidite	1640 CE	100	1905	15
RDL2	82	68.5	10	Turbidite	1245 CE	135	1805	30
RDL3	167	143.5	22	Turbidite	3200	240		
RDL4	193	147.5	8	Turbidite	3335	225		
RDL5	236.5	183	38	Turbidite	4630	540		
RDL6	279	187.5	8.5	Turbidite	4830	590		
<i>COR07-03-11PC</i>								
RDL1	50	50	62.5	Turbidite			1865	25
RDL2	118.5	56	126.5	Debrite			1845	25
<i>COR07-03-13PC</i>								
RDL1	3	3	101.5	Debrite	1650 CE	5		
RDL2	357	354	25	Turbidite				
RDL3	386	358	11.5	Turbidite				
<i>COR20-02-04GC</i>								
RDL1	66.5	66.5	11.5	Turbidite	1665 CE	70		
<i>COR20-02-19GC</i>								
RDL1	44.5	44.5	4	Turbidite	1690 CE	90	1880	20
RDL2	107	103	10.5	Turbidite	1115 CE	140	1700	50
<b>Rimouski</b>								
<i>COR20-02-03GC</i>								
RDL1	57	57	19.5	Turbidite	1870 CE	75		
RDL2	124	104.5	9	Turbidite	1630 CE	60		
<b>Forestville</b>								
<i>COR20-02-20GC</i>								
RDL1	53.5	53.5	73.5	Turbidite	1515 CE	125	1665	35
RDL2	338.5	265	10.5	Turbidite	3155	140		
RDL3	351.5	267.5	28.5	Turbidite	3190	150		
<i>COR20-02-21GC</i>								
RDL1	83.5	83.5	18	Turbidite	1675 CE	115		
RDL2	154	136	19.5	Turbidite	745 CE	140		
RDL3	196	158.5	10.5	Turbidite	325 CE	150		
RDL4	247	199	11	Turbidite	2435	275		

<b>Saguenay</b>						
<i>COR20-02-26GC</i>						
RDL1	4	4	12	Turbidite		2010 5
RDL2	157	145	20	Turbidite		1675 30
RDL3	190	158	66.5	Hyperpycnite		1645 35
<i>COR20-02-28GC-3</i>						
RDL1	50	50	not fully cored	Debrite		1885 10
<i>COR20-02-29GC</i>						
RDL1	34	34	not fully cored	Debrite		1930 5
<b>La Malbaie</b>						
<i>COR20-02-50GC</i>						
RDL1	33.5	33.5	13	Turbidite	1990 CE	5
RDL2	67	54	9	Turbidite		
RDL3	87.5	65.5	13.5	Slump		
RDL4	128.5	93	21.5	Hyperpycnite		
RDL5	161	104	12.5	Turbidite		
RDL6	184	114.5	30	Hyperpycnite		
RDL7	227	127.5	5	Turbidite		

412

#### 413 4.3. Correlation with seismic data

414 A sub-horizontal reflector with strong amplitude was identified at shallow depths (< 2.0 m) on seismic  
415 profiles acquired across the different submarine landslide areas (**Fig. 2**). This reflector drapes the  
416 underlying sediments and is covered by a transparent acoustic facies (**Fig. 2-3**). According to the  
417 description and interpretation made by Cauchon-Voyer *et al.* (2008), the sedimentary deposits of the  
418 submarine landslide triggered by the 1663 CE earthquake were also characterized by the presence of a  
419 high amplitude reflector called R5 by these authors, underlying a transparent facies.

420 Near Rimouski, at the southern side of the Laurentian Channel, a reflector similar to R5 was identified  
421 in seismic profile RIM\_1T (**Fig. 3**) at ~ 1.3 m depth below the deformed seafloor and shows an angular  
422 discordance with deeper, undisturbed reflectors. In the Betsiamites area, R5 type reflector was identified  
423 in seismic profile RIM\_1A that crosses the lobe deposit of Betsiamites (Bernatchez, 2003) at a depth of  
424 ~ 0.75 m below the seafloor (**Fig. 3**). The deeper reflectors R1 to R4 and the seismic units U3 to U5  
425 described by Cauchon-Voyer *et al.* (2008) are also visible and delimited. In seismic profiles BET\_B\_2T,  
426 R5 type reflector is found at a depth of ~ 1.8 mbsf (**Fig. 3**) while further to the south, it is identified at a  
427 depth of ~ 1.2 mbsf in the BET\_D\_2T profile (**Fig. 3**). In the Forestville area, the R5 type reflector is  
428 visible on both sides of the Laurentian Channel at a depth between ~ 1.0 mbsf and ~ 1.3 mbsf, in the  
429 seismic profiles FOR\_A\_1T and ESC\_BCD\_1T (**Fig. 4**). The R5 type reflector is again identified in the  
430 Saguenay area in seismic profile SAG\_H\_1T at about 2.0 mbsf depth (**Fig. 4**).

431 A correlation between sedimentological data and seismic profiles reveals that the R5 type reflector  
432 systematically corresponds to the base of RDLs. Thus, the RDLs correspond to strong sub-horizontal  
433 and parallel reflectors above and at the end of mass-transport deposits characterized by a chaotic and  
434 transparent seismic facies (**Fig. 3-4**). In the Betsiamites area, reflector R5 corresponds to the presence  
435 of turbidite T1 dated to 1665 CE in core COR20-02-04GC. In COR20-02-19GC, R5 corresponds to  
436 turbidite T2 estimated at 1700 CE based on the  $^{210}\text{Pb}$  derived sedimentation rate. Turbidite T3 in core  
437 COR20-02-18GC is also related to reflector R5 and is dated to 1570 CE based on the  $^{210}\text{Pb}$  derived  
438 sedimentation rate. In the Rimouski area, turbidite T2 dated to 1630 CE is at the same depth as the R5  
439 reflector. In Forestville, the turbidites T1 in core COR20-02-20GC and T2 in core COR20-02-21GC,  
440 are respectively dated around 1515-1665 CE and 1675 CE and located at a depth corresponding to that  
441 of reflector R5. Finally, this reflector is at the same depth as turbidites T2 or T3 in core COR20-02-  
442 26GC collected at the mouth of the Saguenay River and dated between 1645 and 1675 CE. The similarity  
443 of these ages with the age interpreted by Cauchon-Voyer *et al.* (2008) confirms that the sub-horizontal  
444 reflectors described in the present study correspond to the seismic reflector R5.

445 A second reflector R6, shallower than R5 (< 1 m) and characterized by a weaker amplitude is observed  
446 in the Betsiamites and Rimouski areas (**Fig. 3**). R6 correlates with the depth of turbidite T2 (~ 0.80 m)  
447 in COR20-02-18GC, turbidite T1 (~ 0.50 m) in core COR20-02-19GC, turbidite T1 or T2 (~ 0.50 – 1.20  
448 m) in core COR07-03-11PC and turbidite T1 (~ 0.60 m) in core COR20-02-03GC. These three turbidites  
449 dated 1805 CE, 1690 - 1880 CE and 1870 CE, respectively.

## 450 **5. Discussion**

### 451 *5.1. Relationship between submarine landslides and rapidly deposited layers (RDL)*

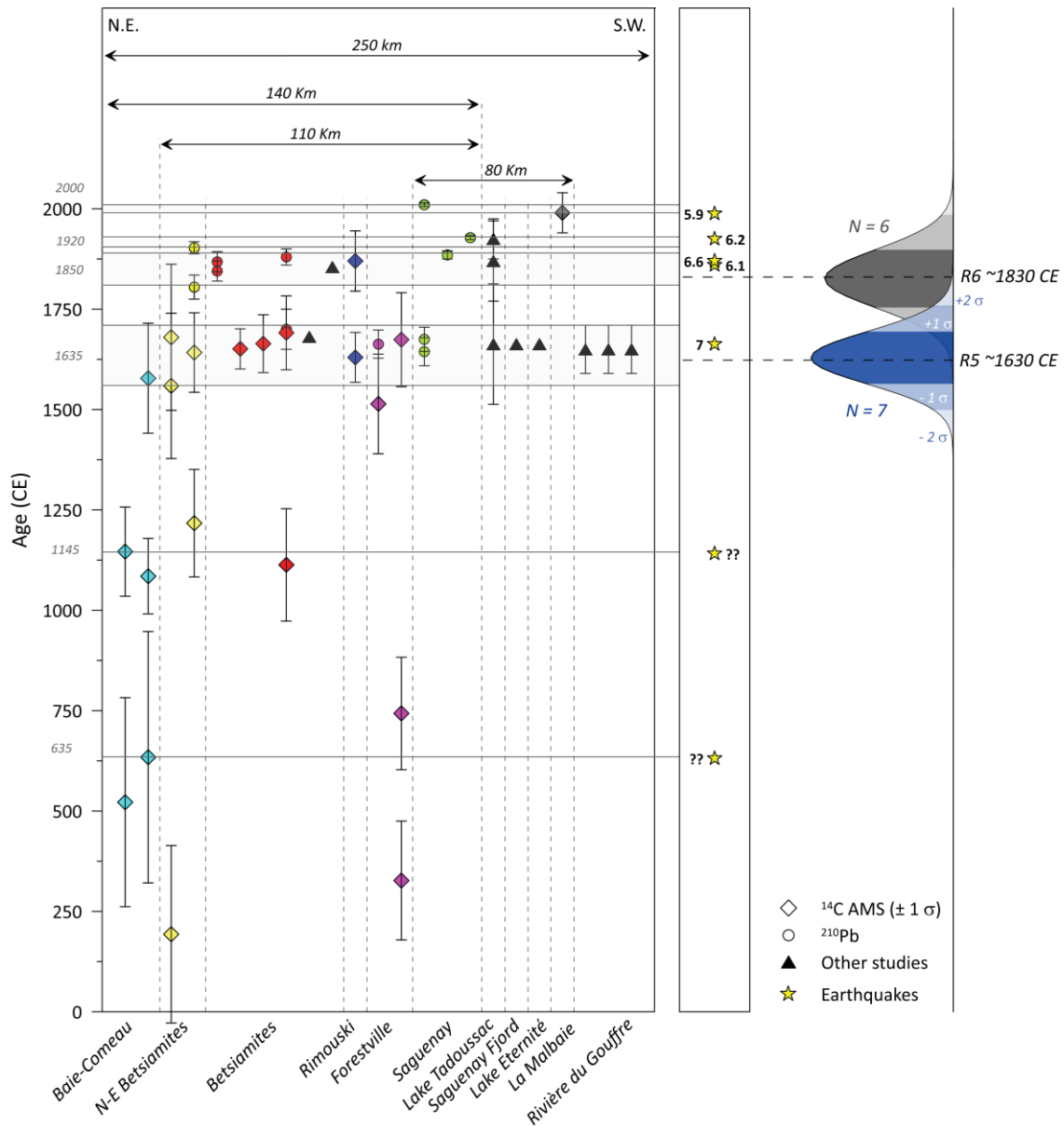
452 The irregularity of deposits and the presence of coarse material and debris in submarine landslides makes  
453 coring difficult. During the SLIDE-2020 expedition, the coring sites were determined in order to  
454 overcome this limitation by targeting sub-horizontal reflectors in the distal part of submarine landslides  
455 where they are thin enough for their underlying and overlying sediments to be dated (e.g., Piper *et al.*,  
456 2019). The relationship between these reflectors and the mass-transport deposits is observed in the  
457 Betsiamites area (seismic profile BET\_D\_2T) and the Saguenay area (seismic profile SAG\_H\_1T)

458 where the R5 reflector corresponding to RDLs is in the continuity with the sliding mass and above  
459 (Strachan, 2008). However, the fact that this geometry is not systematically identified, does not imply  
460 that this genetic link does not exist. Indeed, the coring revealed that the R5 reflector extending over the  
461 Lower Estuary corresponds to RDLs that may have been triggered by a submarine landslide or debris  
462 flow. The large number of turbidites observed in the cores recovered during the SLIDE2020 expedition  
463 validates their correspondence with sub-horizontal seismic reflectors distal to submarine landslides.  
464 Furthermore, it implies that the submarine landslides have progressively transformed into turbidity  
465 currents. The proximal turbidites have a higher proportion of coarse sediment (e.g., T2 in COR20-02-  
466 19GC,  $d_{50} \sim 103 \mu\text{m}$ ) than distal turbidites (e.g., T1 in COR20-02-04GC,  $d_{50} \sim 28 \mu\text{m}$ ) and the cores  
467 recovered from a site very close to mass transport deposits revealed debrites (e.g., COR20-02-29GC)  
468 confirming that the RDLs are deposited by submarine landslides. The fragment of terrestrial soil in  
469 debrite D1 of core COR07-03-13PC which may have been transported by the 1663 CE Colombier event  
470 along coast of the Betsiamites area (see Bernatchez, 2003) tends to support this relationship.

#### 471 *5.2. Chronology of the RDLs and triggering factors*

472 The dated RDLs are assembled in **Fig. 9**. This figure reveals four distinct periods with at least twelve  
473 concomitant submarine landslides at the regional scale. The first period is between 1560 CE and  
474 1710 CE with nine submarine landslides with a mean age of  $1635 \pm 75$  CE spread over 140 km. RDLs  
475 deposited at this period correspond to reflector R5, observed regionally and dated to  $1630 \pm 65$  CE (**Fig.**  
476 **9**). The second period begins at 1800 CE and ends at 1900 CE. It includes six submarine landslides over  
477 a distance of 110 km and RDLs deposited in this period correlate with the seismic reflector R6 dated to  
478  $1830 \pm 70$  CE. The third period spans from 1910 CE to 1930 CE with two submarine landslide in the  
479 Betsiamites area and another 110 km away in the Saguenay. Finally, the fourth period extends from  
480 1990 CE to 2010 CE with two submarine landslides 80 km apart.

481 The dating of RDLs presented in **Table 4** includes ages beyond 2000 years, but they are not included in  
482 the synthesis in **Fig. 9**. Indeed, from ages older than 2000 years, the uncertainties become more  
483 important and it is difficult to establish with certainty that RDLs are synchronous. Moreover, it is not  
484 possible to establish a link between these deposits and historical seismicity.



485

486 **Fig. 9.** Chronology of the RDLs (turbidites and debrites) dated by  $^{14}\text{C}$  (colored diamonds) and  $^{210}\text{Pb}$   
 487 (colored circles). The black triangles correspond to evidences provided by previous studies of aerial or  
 488 submarine landslides in Québec (Doig, 1990, Filion *et al.*, 1990, St-Onge *et al.*, 2004, Cauchon-Voyer  
 489 *et al.*, 2008, Locat *et al.*, 2016). The gray intervals highlight periods of synchronous RDLs. The black  
 490 arrows show the distance of synchronous submarine landslides for each period. The yellow stars indicate  
 491 the timing of major historical earthquakes with their magnitude. To the right, the range of reflectors R5  
 492 (blue) and R6 (gray) considering a statistical error of  $\pm 1\sigma$  and  $\pm 2\sigma$ .

493 During the four periods identified, four to five major historical earthquakes occurred in the St. Lawrence  
 494 Estuary region (Lamontagne *et al.*, 2018): 1663 ( $M \leq 7$ ), 1860 ( $M = 6.1$ ) or 1870 ( $M = 6.6$ ), 1925 ( $M =$   
 495  $6.2$ ) and 1988 ( $M = 5.9$ ) (**Table 5**). The difference between the  $^{14}\text{C}$  ages and ages calculated from  
 496 sedimentation rates for the different RDLs may be related to the accuracy of the dating method and RDL  
 497 thickness measurements. The most accurate cases correspond to turbidites T1 in cores COR20-02-04GC  
 498 and COR20-02-20GC. Indeed, in core COR20-02-04GC, turbidite T1 is already considered to be  
 499 associated with the 1663 CE earthquake by Cauchon-Voyer *et al.* (2008) and has been dated at 1665 CE  
 500 based on  $^{14}\text{C}$  dating of the immediately underlying hemipelagic deposits. The  $^{210}\text{Pb}$  dating of turbidite  
 501 T1 in core COR20-02-20GC yields an age of  $1665 \pm 35$  CE, in agreement with the  $^{14}\text{C}$  age considering  
 502 the dating uncertainties ( $1515 \text{ CE} \pm 125$  at  $1\sigma$  and  $1515 \text{ CE} \pm 245$  at  $2\sigma$ ). The density profiles obtained  
 503 with the MSCL and from water content measurements do not show a linear evolution with depth, but a  
 504 rather stable density over the upper 2 m, suggesting that compaction can be neglected for the age  
 505 calculations of the RDL with  $^{210}\text{Pb}$ -derived sedimentation rates. The reliability of these dates supports  
 506 the correlation between submarine landslides and historical seismicity but the close age of the 1860 and  
 507 1870 CE earthquakes does not lend to differentiate these events from our chronology owing to the age  
 508 uncertainty of the dated RDLs.

509 **Table 5.** List of major historical earthquakes in the St. Lawrence Estuary (from Lamontagne *et al.*,  
 510 2018).

Year	Lat (°N)	Long (°W)	Area	Magnitude	MMI	Magnitude information	Source
1663	47.60	-70.10	Charlevoix-Kamouraska	7.0	IX	Estimated	Gouin, 2001
1860	47.50	-70.10	Charlevoix-Kamouraska	6.1	VIII	Estimated	Gouin, 2001
1870	47.40	-70.50	Charlevoix-Kamouraska	6.6	IX-X	Estimated	Gouin, 2001
1925	47.80	-69.80	Charlevoix-Kamouraska	6.2	VIII	Instrumented	Hodgson, 1950; Bruneau & Lamontagne, 1994
1988	48.12	-71.18	Saguenay Region	5.9	VIII	Instrumented	North <i>et al.</i> , 1989

511 Submarine landslides triggered by earthquakes have already been described in other regions of the world  
 512 (e.g., Bryn *et al.*, 2005; Dan *et al.*, 2009). Ground shaking during an earthquake constitutes a major

513 factor for slope destabilisation (Hampton *et al.*, 1996) and its influence can exceed several hundreds of  
514 kilometers to trigger several independent failures (Goldfinger *et al.*, 2012, 2017). The synchronicity  
515 between RDLs in a seismic region is increasingly used for the study of paleoseismicity during the  
516 Holocene (Goldfinger *et al.*, 2007, Gracia *et al.*, 2010, Ratsov *et al.*, 2015, Howarth *et al.*, 2021). Storms,  
517 river floods and rapid relative sea level rise can also trigger submarine landslides and turbidites at the  
518 regional scale (~ 100 km) (Talling, 2014). However, the RDLs in this study were not connected to river  
519 mouths. At the scale of the last 500 years, relative sea level variations are insignificant (Dionne, 2001;  
520 Shaw *et al.*, 2002; Remillard *et al.*, 2017). Storms in eastern Canada are much weaker than tropical  
521 storms (e.g., Taiwan, New-Zealand) and the physiography of the estuary allows it to be relatively  
522 sheltered from oceanic swells (Bernatchez *et al.*, 2012). Therefore, the synchronicity of submarine  
523 landslides that are reported here over a large area of a known seismic zone is a strong argument for  
524 relating their triggering to the regional seismicity of the CKBSL seismic zone.

525 The RDL 3 observed in core COR20-02-26GC and dated around 1645 CE in the Saguenay area is  
526 interpreted as a hyperpycnite. In the Saguenay Fjord, St-Onge *et al.* (2004) and Syvitski and Schafer  
527 (1996) describe a similar deposit related to the 1663 CE earthquake. It was interpreted as a flood-induced  
528 hyperpycnal flow after the breach of a natural dam generated by an earthquake-triggered turbidite.  
529 Historical observations reported by the Jesuit mission and synthesized by Gouin (2001) support the  
530 generation of a hyperpycnal flow by the 1663 CE earthquake in the Saguenay area (e.g., Tadoussac) and  
531 throughout the estuary : “*Rivers were thoroughly polluted, the waters of some becoming yellow and of*  
532 *others red; and our great river St. Lawrence appeared all whitish as far as the region of Tadoussacq*”;  
533 *“displaced lands [...] caused their gradual detrition by the water of the Rivers, which are still so thick*  
534 *and turbid as to change the colour of the whole great St. Lawrence river.”*

535 In the Middle Estuary, the tidal range and currents are stronger (Saucier and Chassé, 2000) as evidenced  
536 by the coarser sediments composing the hemipelagites observed in core COR20-02-50GC. These  
537 forcings, particularly effective at low water depths could play a major role in preconditioning submarine  
538 landslides in the CKSZ, as currents can erode submarine slopes causing oversteepening (Hampton *et*  
539 *al.*, 1996). These preconditioning factors combined with the high seismicity of the CKSZ (Lamontagne

540 *et al.*, 2018) could increase the submarine landslide hazard in the Middle Estuary, which in turn could  
541 explain the high frequency of RDL observed in core COR20-02-50GC (four turbidites, two  
542 hyperpycnites and one slump). Moreover, the 1663 CE earthquake may have occurred in this region  
543 (*Lamontagne et al.*, 2018).

### 544 5.3. Relative importance of the 1663 CE event

545 The 1663 CE earthquake was the strongest historical earthquake in Eastern Canada (*Locat et al.*, 2003;  
546 *Ebel*, 2011; *Lamontagne et al.*, 2018). This statement is confirmed by our study that allowed identifying  
547 at least 12 RDLs dated at ~1663 CE in 10 sediment cores distributed over a distance of 140 km, whereas  
548 only five RDLs dated at ~1860/1870 CE and two at ~1925 CE and ~1988 CE were observed over a less  
549 extensive area. The seismic survey revealed a strong shallow reflector present in almost all the studied  
550 area in the slopes and in the submarine landslide deposits. Intersecting cores analyzed and dated this  
551 reflector R5 (**Fig. 3-4**). Its approximate age is near to that of the 1663 CE earthquake. A second reflector  
552 has been identified (R6) and dated at about 1830 – 1860 CE, which is very close to the two other major  
553 historical earthquakes of 1860 and 1870 CE (**Fig. 3**). Shallower than R5, this seismic reflector is  
554 identified at fewer locations, confirming the relative importance of the 1663 CE earthquake compared  
555 to more recent events such as the 1860 and 1870 CE earthquakes.

556 In this study, it thus appears that the 1663 CE earthquake has triggered more submarine landslides over  
557 a larger area than more recent earthquakes (**Fig. 9**), attesting to the importance of this event at the scale  
558 of the last two millennia and corroborating historical observations reported by the first European settlers  
559 (*Gouin*, 2001, *Ebel*, 2011). Other studies in Québec (*Doig*, 1990, *Filion et al.*, 1991, *St-Onge et al.*,  
560 2004; *Cauchon-Voyer et al.*, 2008, *Poncet et al.*, 2010; *Locat et al.*, 2016) highlight the highest intensity  
561 of this major event. In comparison, more recent earthquakes (**Table 5**) appear to have had less impact  
562 than the 1663 CE earthquake. However, the relation between earthquake magnitude and the number of  
563 submarine landslides is not linear (e.g., *Papadopoulos and Plessa*, 2000). Some factors can interfere such  
564 as the sedimentary budget and predisposing factors (*Hampton et al.*, 1996).

565 The compilation of submarine landslide ages leads to identify two older periods with synchronous ages  
566 of RDLs. The first at  $1145 \pm 145$  CE with four synchronous deposits distributed over a distance of 40 km



567 and the second at  $645 \pm 400$  CE with three synchronous RDLs over a distance of 100 km. The first  
568 period has already been identified by Philibert *et al.* (2012) by the dating of RDL at  $\sim 1200$  CE in Lake  
569 Jacques-Cartier (**Fig. 1**) and correlated with the seismicity of CKSZ. Moreover, Normandeau *et al.*  
570 (2013) found an earthquake-triggered submarine landslide deposit in Lake St-Joseph (**Fig. 1**) dated at  
571  $\sim 1250$  CE. Trottier *et al.* (2019) in Lake Maskinongé (CKSZ) also identified mass transport deposits  
572 about the same period at  $\sim 1180$  CE through geomorphic and core analyses. Additionally, the major event  
573 identified and dated around 650 CE by Lajeunesse *et al.*, (2017) in Lake Témiscouata near the  
574 Charlevoix area is likely synchronous with the RDLs dated at  $645 \pm 400$  CE period in this study. The  
575 link between regional seismicity and the submarine landslides established in addition to these studies  
576 tends to suggest that two earthquakes could have triggered these older RDLs in the St. Lawrence Estuary.

## 577 **6. Conclusions**

578 The dating of 12 submarine landslides distributed over a distance of 220 km along the axis of the St.  
579 Lawrence Estuary allowed correlating them to the major historical earthquakes of 1663 CE, 1860 and/or  
580 1870 CE and 1925 CE. The observation of older submarine landslide deposits suggests that two large  
581 earthquakes may have occurred around 645 CE and 1145 CE, in a period when historical data are not  
582 available. The criteria used to infer these relationships are:

- 583 1) The careful location of the coring sites outside areas influenced by storms, sediment input (e.g.,  
584 rivers) and active turbiditic channels;
- 585 2) The  $^{14}\text{C}$  and  $^{210}\text{Pb}$  dating of turbidites and debrites revealing concomitant ages with the historical  
586 earthquakes;
- 587 3) The synchronicity of submarine landslides and their associated turbidites described over a  
588 distance of  $\sim 220$  km in a seismically active zone;

589 The results reported in this paper provide evidence that allow estimating the paleoseismicity of the last  
590 2000 years in the St. Lawrence Estuary, which in turn improves the seismic hazard assessment in Eastern  
591 Canada. These results also allow demonstrating that the 1663 CE earthquake was the most important  
592 event of the last two millennia, although several submarine landslides observed in this study still remain  
593 to be dated. Investigating in detail these landslides would allow going even further back into the

594 paleoseismological archives, refining the location of the epicenter of the 1663 CE earthquake and assess  
595 landslide-related hazards. Additionally, characterizing of the mechanical behavior of sediments  
596 recovered in the St. Lawrence Estuary could help in evaluating the stability of slopes during an  
597 earthquake with specific attention on the stratified seismic unit 4, which seems susceptible to failure.  
598 Additional investigations are needed to characterize and understand the behavior and role of this unit  
599 during an earthquake, in particular its liquefaction potential.

## 600 **Acknowledgements**

601 The authors wish to thank the captain and crew of the SLIDE2020 expedition on board the RV Coriolis  
602 II. They also thank Quentin Beauvais, Pascal Rioux and Sandrine Ouellet (ISMER) for their help in the  
603 laboratory, as well as Ray Burke for his contribution in the acquisition of geophysical data. The  
604 SLIDE2020 expedition was supported by ship time of the *Odyssée Saint-Laurent* program of the *Réseau*  
605 *Québec maritime* (RQM). G. St-Onge and P. Lajeunesse gratefully acknowledge the financial support  
606 of the Natural Sciences and Engineering Research Council of Canada (NSERC). Finally, the authors  
607 thank the two anonymous reviewers for their comments, which improved the quality of this paper.

## References

- Adams, J., Basham, P., 1989. The seismicity and seismotectonics of Canada east of the Cordillera. *Geoscience Canada* 16, 3-16.
- Anglin, F., 1984. Seismicity and faulting in the Charlevoix zone of the St. Lawrence Valley. *Bulletin of the Seismological Society of America* 74, 595-603.
- Appleby, P.G., Oldfield, F., 1978. The calculation of lead-210 dates assuming a constant rate of supply of unsupported  $^{210}\text{Pb}$  to the sediment. *Catena* 5, 1-8.
- Bernatchez, P., 2003. Évolution littorale holocène et actuelle des complexes deltaïques de Betsiamites et de Manicouagan-Outardes: synthèse, processus, causes et perspectives.
- Bernatchez, P., Boucher-Brossard, G., Sigouin-Cantin, M., 2012. Contribution des archives à l'étude des événements météorologiques et géomorphologiques causant des dommages aux côtes du Québec maritime et analyse des tendances, des fréquences et des temps de retour des conditions météorologiques extrêmes. Rapport remis au ministère de la Sécurité publique du Québec. Chaire de recherche en géoscience côtière, Laboratoire de dynamique et de gestion intégrée des zones côtières, Université du Québec à Rimouski, Rimouski.
- Blaauw, M., Christen, J.A., 2011. Flexible paleoclimate age-depth models using an autoregressive gamma process. *Bayesian analysis* 6, 457-474.
- Bouma, A.H., 1962. Sedimentology of some flysch deposits. *Graphic approach to facies interpretation* 168.
- Bruneau, M., Lamontagne, M., 1994. Damage from 20th century earthquakes in eastern Canada and seismic vulnerability of unreinforced masonry buildings. *Canadian Journal of Civil Engineering* 21, 643-662.
- Bryn, P., Berg, K., Forsberg, C.F., Solheim, A., Kvalstad, T.J., 2005a. Explaining the Storegga slide. *Marine and Petroleum Geology* 22, 11-19.
- Cauchon-Voyer, G., Locat, J., Leroueil, S., St-Onge, G., Demers, D., 2011. Large-scale subaerial and submarine Holocene and recent mass movements in the Betsiamites area, Quebec, Canada. *Engineering Geology* 121, 28-45.
- Cauchon-Voyer, G., Locat, J., St-Onge, G., 2008. Late-Quaternary morpho-sedimentology and submarine mass movements of the Betsiamites area, Lower St. Lawrence Estuary, Quebec, Canada. *Marine Geology* 251, 233-252.
- Cauchon-Voyer, G., Turmel, D., Gagné, H., 2007. Rapport de mission COR0703, Estuaire du Saint-Laurent.
- Croudace, I.W., Rindby, A., Rothwell, R.G., 2006. ITRAX: description and evaluation of a new multi-function X-ray core scanner. *Geological Society, London, Special Publications* 267, 51-63.
- Dan, G., Sultan, N., Savoye, B., Deverchere, J., Yelles, K., 2009. Quantifying the role of sandy-silty sediments in generating slope failures during earthquakes: example from the Algerian margin. *International Journal of Earth Sciences* 98, 769-789.

- Dionne, J.-C., 2001. Relative-sea-level changes in the St. Lawrence Estuary from deglaciation to present day. *Deglacial history and relative sea-level changes, northern New England and adjacent Canada* 351, 271-284.
- Doig, R., 1990. 2300 yr history of seismicity from silting events, in Lake Tadoussac, Charlevoix, Quebec. *Geology* 18, 820-823.
- Dubé, S., 1998. Analyse de l'éroulement rocheux du Mont Éboulé,(Québec).
- Duchesne, M., Pinet, N., Bolduc, A., Bédard, K., Lavoie, D., 2007. Seismic stratigraphy of the lower St Lawrence River estuary (Quebec) Quaternary deposits and seismic signature of the underlying geological domains. *Geological Survey of Canada*.
- Duchesne, M.J., Pinet, N., Bédard, K., St-Onge, G., Lajeunesse, P., Campbell, D.C., Bolduc, A., 2010. Role of the bedrock topography in the Quaternary filling of a giant estuarine basin: the Lower St. Lawrence Estuary, Eastern Canada. *Basin Research* 22, 933-951.
- Ebel, J.E., 1996. The seventeenth century seismicity of northeastern North America. *Seismological Research Letters* 67, 51-68.
- Ebel, J.E., 2011. A new analysis of the magnitude of the February 1663 earthquake at Charlevoix, Quebec. *Bulletin of the Seismological Society of America* 101, 1024-1038.
- Filion, L., Quinty, F., Bégin, C., 1991. A chronology of landslide activity in the valley of Rivière du Gouffre, Charlevoix, Quebec. *Canadian Journal of Earth Sciences* 28, 250-256.
- Goldfinger, C., Galer, S., Beeson, J., Hamilton, T., Black, B., Romsos, C., Patton, J., Nelson, C.H., Hausmann, R., Morey, A., 2017. The importance of site selection, sediment supply, and hydrodynamics: A case study of submarine paleoseismology on the northern Cascadia margin, Washington USA. *Marine Geology* 384, 4-46.
- Goldfinger, C., Morey, A.E., Nelson, C.H., Gutiérrez-Pastor, J., Johnson, J.E., Karabanov, E., Chaytor, J., Eriksson, A., Party, S.S., 2007. Rupture lengths and temporal history of significant earthquakes on the offshore and north coast segments of the Northern San Andreas Fault based on turbidite stratigraphy. *Earth and Planetary Science Letters* 254, 9-27.
- Goldfinger, C., Nelson, C.H., Morey, A.E., Johnson, J.E., Patton, J.R., Karabanov, E.B., Gutierrez-Pastor, J., Eriksson, A.T., Gracia, E., Dunhill, G., 2012. Turbidite event history—Methods and implications for Holocene paleoseismicity of the Cascadia subduction zone. *US Geological Survey*.
- Gracia, E., Vizcaino, A., Escutia, C., Asioli, A., Rodes, A., Pallas, R., Garcia-Orellana, J., Lebreiro, S., Goldfinger, C., 2010. Holocene earthquake record offshore Portugal (SW Iberia): testing turbidite paleoseismology in a slow-convergence margin. *Quaternary Science Reviews* 29, 1156-1172.
- Hampton, M.A., Lee, H.J., Locat, J., 1996. Submarine landslides. *Reviews of geophysics* 34, 33-59.
- Haworth, R.T., 1978. Interpretation of geophysical data in the northern Gulf of St. Lawrence and its relevance to lower Paleozoic geology. *Geological Society of America Bulletin* 89, 1091-1110.
- Heaton, T.J., Köhler, P., Butzin, M., Bard, E., Reimer, R.W., Austin, W.E., Ramsey, C.B., Grootes, P.M., Hughen, K.A., Kromer, B., 2020. Marine20—the marine radiocarbon age calibration curve (0–55,000 cal BP). *Radiocarbon* 62, 779-820.

- Hodgson, E., 1928. The Probable Epicentre of the Saint Lawrence Earthquake of Feb. 5 1663. *Journal of the Royal Astronomical Society of Canada* 22, 325.
- Hodgson, E.A., 1925. The Saint Lawrence earthquake March 1, 1925. *Publications of the Dominion Observatory Ottawa* 7, 363-436.
- Howarth, J.D., Orpin, A.R., Kaneko, Y., Strachan, L.J., Nodder, S.D., Mountjoy, J.J., Barnes, P.M., Bostock, H.C., Holden, C., Jones, K., 2021. Calibrating the marine turbidite palaeoseismometer using the 2016 Kaikōura earthquake. *Nature Geoscience* 14, 161-167.
- Jaegle, M., 2015. *Nature et origine des sédiments de surface de l'estuaire du Saint-Laurent*. Université du Québec à Rimouski.
- Josenhans, H., Lehman, S., 1999. Late glacial stratigraphy and history of the Gulf of St. Lawrence, Canada. *Canadian Journal of Earth Sciences* 36, 1327-1345.
- King, L.H., MacLean, B., 1970. Origin of the outer part of the Laurentian Channel. *Canadian Journal of Earth Sciences* 7, 1470-1484.
- Lajeunesse, P., Sinkunas, B., Morissette, A., Normandeau, A., Joyal, G., St-Onge, G., Locat, J., 2017. Large-scale seismically-induced mass-movements in a former glacial lake basin: Lake Témiscouata, northeastern Appalachians (eastern Canada). *Marine Geology* 384, 120-130.
- Lamontagne, M., 2000. Rheological and geological constraints on the earthquake distribution in the Charlevoix Seismic Zone, Quebec, Canada.
- Lamontagne, M., Beauchemin, M., Toutin, T., 2003. Earthquakes in the Charlevoix seismic zone, Quebec. *International Journal on Hydropower & Dams* 10, 98-99.
- Lamontagne, M., Halchuk, S., Cassidy, J., Rogers, G., 2008. Significant Canadian earthquakes of the period 1600–2006. *Seismological Research Letters* 79, 211-223.
- Lamontagne, M., Halchuk, S., Cassidy, J.F., Rogers, G.C., 2018. Significant Canadian earthquakes 1600-2017. Geological Survey of Canada.
- Lasalle, P., Chagnon, J.-Y., 1968. An ancient landslide along the Saguenay River, Quebec. *Canadian Journal of Earth Sciences* 5, 548-549.
- Lebreiro, S.M., McCave, I.N., Weaver, P.P., 1997. Late Quaternary turbidite emplacement on the Horseshoe abyssal plain (Iberian margin). *Journal of Sedimentary Research* 67, 856-870.
- Lee, K.L., 1979. Cyclic strength of a sensitive clay of eastern Canada. *Canadian Geotechnical Journal* 16, 163-176.
- Locat, J., 2011. La localisation et la magnitude du séisme du 5 février 1663 (Charlevoix) revues à l'aide des mouvements de terrain. *Canadian Geotechnical Journal* 48, 1266-1286.
- Locat, J., Martin, F., Levesque, C., Locat, P., Leroueil, S., Konrad, J.-M., Urgeles, R., Canals, M., Duchesne, M., 2003. Submarine mass movements in the upper Saguenay Fjord, (Québec, Canada), triggered by the 1663 earthquake, Submarine mass movements and their consequences. Springer, pp. 509-519.

- Locat, J., Turmel, D., Habersetzer, M., Trottier, A.-P., Lajeunesse, P., St-Onge, G., 2016. Earthquake induced landslides in Lake Eternité, Québec, Canada, Submarine Mass Movements and their Consequences. Springer, pp. 361-370.
- Martin, F., Konrad, J.-M., Locat, J., Locat, P., Urgeles, R., Lee, H., CARACTERISTIQUES GEOTECHNIQUES ET ANALYSE DU POTENTIEL DE LIQUEFACTION DES SEDIMENTS RECENTS ET POST-GLACIAIRES DU FJORD DU SAGUENAY, QUEBEC (CANADA).
- McNeely, R., Dyke, A.S., Southon, J.R., 2006. Canadian marine reservoir ages preliminary data assessment. Geological Survey of Canada.
- Mulder, T., Syvitski, J.P., Migeon, S., Faugères, J.-C., Savoye, B., 2003. Marine hyperpycnal flows: initiation, behavior and related deposits. A review. *Marine and Petroleum Geology* 20, 861-882.
- Normandeau, A., Dietrich, P., Lajeunesse, P., St-Onge, G., Ghienne, J.-F., Duchesne, M.J., Francus, P., 2017. Timing and controls on the delivery of coarse sediment to deltas and submarine fans on a formerly glaciated coast and shelf. *GSA Bulletin* 129, 1424-1441.
- Normandeau, A., Lajeunesse, P., Philibert, G., 2013. Late-Quaternary morphostratigraphy of Lake St-Joseph (southeastern Canadian Shield): Evolution from a semi-enclosed glacial marine basin to a postglacial lake. *Sedimentary Geology* 295, 38-52.
- Normandeau, A., Lajeunesse, P., St-Onge, G., 2015. Submarine canyons and channels in the Lower St. Lawrence Estuary (Eastern Canada): Morphology, classification and recent sediment dynamics. *Geomorphology* 241, 1-18.
- North, R.G., Wetmiller, R.J., Adams, J., Anglin, F.M., Hasegawa, H.S., Lamontagne, M., Berger, R.D., Seeber, L., Armbruster, J., 1989. Preliminary results from the November 25, 1988 Saguenay (Quebec) earthquake. *Seismological Research Letters* 60, 89-93.
- Obermeier, S.F., Martin, J., Frankel, A., Youd, T., Munson, P., Munson, C., Pond, E., 1992. Liquefaction evidence for strong Holocene earthquake (s) in the Wabash Valley of southern Indiana-Illinois, with a preliminary estimate of magnitude. US Department of the Interior, US Geological Survey.
- Ouellet, M., 1997. Lake sediments and Holocene seismic hazard assessment within the St. Lawrence Valley, Québec. *Geological Society of America Bulletin* 109, 631-642.
- Papadopoulos, G.A., Plessa, A., 2000. Magnitude–distance relations for earthquake-induced landslides in Greece. *Engineering Geology* 58, 377-386.
- Patton, J.R., Goldfinger, C., Morey, A.E., Ikehara, K., Romsos, C., Stoner, J., Djadjadihardja, Y., Ardhyastuti, S., Gaffar, E.Z., Vizcaino, A., 2015. A 6600 year earthquake history in the region of the 2004 Sumatra-Andaman subduction zone earthquake. *Geosphere* 11, 2067-2129.
- Philibert, G., 2012. Évolution tardi-quaternaire du lac Jacques-Cartier, Réserve faunique des Laurentides, Québec.
- Pinet, N., Brake, V., Campbell, C., Duchesne, M., 2011. Seafloor and shallow subsurface of the St. Lawrence River Estuary. *Geoscience Canada* 38, 31-40.

- Pinet, N., Brake, V., Campbell, C., Duchesne, M.J., 2015. Geomorphological characteristics and variability of Holocene mass-transport complexes, St. Lawrence River Estuary, Canada. *Geomorphology* 228, 286-302.
- Pinet, N., Duchesne, M., Lavoie, D., Bolduc, A., Long, B., 2008. Surface and subsurface signatures of gas seepage in the St. Lawrence Estuary (Canada): significance to hydrocarbon exploration. *Marine and Petroleum Geology* 25, 271-288.
- Pinet, N., Lamontagne, M., Duchesne, M.J., Brake, V.I., 2021. Hunting for Quaternary faults in eastern Canada: A critical appraisal of two potential candidates. *Seismological Society of America* 92, 1102-1111.
- Piper, D.J., Tripsanas, E., Mosher, D.C., MacKillop, K., 2019. Paleoseismicity of the continental margin of eastern Canada: rare regional failures and associated turbidites in Orphan Basin. *Geosphere* 15, 85-107.
- Poncet, R., Campbell, C., Dias, F., Locat, J., Mosher, D., 2010a. A study of the tsunami effects of two landslides in the St. Lawrence estuary, *Submarine Mass Movements and Their Consequences*. Springer, pp. 755-764.
- Poncet, R., Campbell, C., Dias, F., Locat, J., Mosher, D., 2010b. A study of the tsunami effects of two landslides in the St. Lawrence estuary, *Submarine Mass Movements and Their Consequences*. Springer, pp. 755-764.
- Riboulot, V., Cattaneo, A., Sultan, N., Garziglia, S., Ker, S., Imbert, P., Voisset, M., 2013. Sea-level change and free gas occurrence influencing a submarine landslide and pockmark formation and distribution in deepwater Nigeria. *Earth and Planetary Science Letters* 375, 78-91.
- Roy, D.W., DuBerger, R., 1983. Relations possibles entre la microseismicité récente et l'astroblème de Charlevoix. *Canadian Journal of Earth Sciences* 20, 1613-1618.
- Rémillard, A.M., St-Onge, G., Bernatchez, P., Héту, B., Buylaert, J.-P., Murray, A.S., Lajeunesse, P., 2017. Relative sea-level changes and glacio-isostatic adjustment on the Magdalen Islands archipelago (Atlantic Canada) from MIS 5 to the late Holocene. *Quaternary Science Reviews* 171, 216-233.
- Saucier, F.J., Chassé, J., 2000. Tidal circulation and buoyancy effects in the St. Lawrence Estuary. *Atmosphere-Ocean* 38, 505-556.
- Seed, H.B., Idriss, I.M., 1967. Analysis of soil liquefaction: Niigata earthquake. *Journal of the Soil Mechanics and Foundations Division* 93, 83-108.
- Shaw, J., Gareau, P., Courtney, R., 2002. Palaeogeography of Atlantic Canada 13–0 kyr. *Quaternary Science Reviews* 21, 1861-1878.
- Smith, W.T., 1962. Earthquakes of eastern Canada and adjacent areas, 1534-1927. Department of Energy, Mines and Resources, Observatories Branch.
- St-Onge, G., Lajeunesse, P., Duchesne, M.J., Gagne, H., 2008. Identification and dating of a key Late Pleistocene stratigraphic unit in the St. Lawrence Estuary and Gulf (Eastern Canada). *Quaternary Science Reviews* 27, 2390-2400.

- St-Onge, G., Mulder, T., Francus, P., Long, B., 2007. Chapter two continuous physical properties of cored marine sediments. *Developments in marine geology* 1, 63-98.
- St-Onge, G., Mulder, T., Piper, D.J., Hillaire-Marcel, C., Stoner, J.S., 2004. Earthquake and flood-induced turbidites in the Saguenay Fjord (Québec): a Holocene paleoseismicity record. *Quaternary Science Reviews* 23, 283-294.
- St-Onge, G., Stoner, J.S., Hillaire-Marcel, C., 2003. Holocene paleomagnetic records from the St. Lawrence Estuary, eastern Canada: centennial-to millennial-scale geomagnetic modulation of cosmogenic isotopes. *Earth and Planetary Science Letters* 209, 113-130.
- Strachan, L.J., 2008. Flow transformations in slumps: a case study from the Waitemata Basin, New Zealand. *Sedimentology* 55, 1311-1332.
- Stuiver, M., Reimer, P.J., 1993. Extended 14C data base and revised CALIB 3.0 14C age calibration program. *Radiocarbon* 35, 215-230.
- Syvitski, J., Praeg, D., 1989. Quaternary sedimentation in the St. Lawrence Estuary and adjoining areas, Eastern Canada: An overview based on high-resolution seismo-stratigraphy. *Géographie physique et Quaternaire* 43, 291-310.
- Syvitski, J.P., Schafer, C.T., 1996a. Evidence for an earthquake-triggered basin collapse in Saguenay Fjord, Canada. *Sedimentary Geology* 104, 127-153.
- Syvitski, J.P., Schafer, C.T., 1996b. Evidence for an earthquake-triggered basin collapse in Saguenay Fjord, Canada. *Sedimentary Geology* 104, 127-153.
- Talling, P.J., 2014. On the triggers, resulting flow types and frequencies of subaqueous sediment density flows in different settings. *Marine Geology* 352, 155-182.
- Trottier, A.-P., Lajeunesse, P., Normandeau, A., Gagnon-Poiré, A., 2019. Deglacial and postglacial paleoseismological archives in mass movement deposits of lakes of south-central Québec. *Canadian Journal of Earth Sciences* 56, 60-76.
- Tuttle, M.P., Atkinson, G.M., 2010. Localization of large earthquakes in the Charlevoix seismic zone, Quebec, Canada, during the past 10,000 years. *Seismological Research Letters* 81, 140-147.
- Wu, P., 1998. Intraplate earthquakes and post-glacial rebound in eastern Canada and Northern Europe. *Dynamics of the Ice Age Earth: A Modern Perspective*, 603-628.
- Zhang, D., 2000. Flux de radio-isotopes à courte période dans les bassins marins marginaux de l'est canadien. Ph. D. thesis, Université du Québec à Montréal, Montréal, Québec.